NUMERICAL INVESTIGATION OF PUMPING POWER MINIMIZATION FOR COOLANT CIRCULATION IN SINUSOIDAL CHANNELS

A Thesis Submitted to
the Graduate School of Engineering and Science of
İzmir Institute of Technology
in Partial Fulfillment of the Requirements for the Degree of

MASTER OF SCIENCE

in Energy Engineering

by
Ali AKÇA

November, 2013
İZMİR

We approve the thesis of **Ali AKÇA**

Examining Committee Members:

Assist. Prof. Dr. Ünver ÖZKOL
Department of Mechanical Engineering, İzmir Institute of Technology

Prof. Dr. Gülden GÖKÇEN AKKURT
Department of Mechanical Engineering, İzmir Institute of Technology

Assoc. Prof. Dr. Tahsin BAŞARAN
Department of Architecture, İzmir Institute of Technology

7 November 2013

Assist. Prof. Dr. Ünver ÖZKOL
Supervisor
Department of Mechanical Engineering
İzmir Institute of Technology

Assoc. Prof. Dr. Moghtada MOBEDİ
Co-Supervisor
Department of Mechanical Engineering
İzmir Institute of Technology

Prof. Dr. Gülden GÖKÇEN AKKURT
Head of the Department of
Energy Engineering

Prof. Dr. R. Tuğrul SENGER
Dean of the Graduate School of
Engineering and Sciences

ACKNOWLEDGMENTS

I would like to express my sincere gratitude to my supervisor Assist. Prof. Dr. Ünver ÖZKOL for his valuable advises and guidance through the thesis.

I would like to thank to my best friend Veysel Egemen AĞAKAY in Izmir. I am sure that this thesis would not be completed without his valuable support and friendship.

All members of Fluid Mechanics Laboratory, especially, Ömer Buğra KANARGI and Mustafa Ali BAYTAŞ played great roles in my studies. They were always near me when I need their help.

I would like to express my gratitude to my father. He encouraged me to be member of Izmir Institute of Technology. Thank you very much for what I have in my life. We miss you and never forget you.

Lastly, I would like to thank my dear mother and sister, they have always encouraged and supported me.

ABSTRACT

NUMERICAL INVESTIGATION OF PUMPING POWER MINIMIZATION FOR COOLANT CIRCULATION IN SINUSOIDAL CHANNELS

The electronic devices consume more energy with the increasing their process capacity. Therefore, their temperature increase and unless they are cooled down sufficiently, electronic devices exceed the safety operating temperature and break down. Improvements in electronic technology are obtained as this heat transfer bottleneck is overcome. Moreover, this cooling system consumes electric power as well and this should be minimized. In this thesis, minimization study of the consumed energy to cool down an electronic device is carried out.

In this study, the heat transfer in the rectangular cross-sectional sinusoidal wavy channels is investigated numerically and heat transfer augmentation is considered with reference to a straight channel geometry. Minimization of the surface temperature and the pump power are elaborated for the different wave amplitudes and wavelengths in the channel. The flow in the channel is conducted at the range of Re numbers from 7 to 368 and it assumed laminar and steady state condition. Dissipating heat flux from the electronic module is assumed to be constant. Thermal performance is calculated with observing of the temperature of the critic device on the electronic module and the pump power is evaluated by utilizing pressure drop calculations in the channel. To investigate how the sinusoidal wavy channel affects the cold plate compared to the straight channel, some dimensionless numbers are defined and the assessments are done in accordance with these numbers.

Generally, it was observed that, sinusoidal wavy channel contributes the heat transfer enhancement. While wave amplitude affects heat transfer positively, pump power is affected adversely. Wavelength effect is not important comparing with wave amplitude for the augmentation of heat transfer performance. Nevertheless, it was observed that the increasing the wavelength causes to decrease pump power.

ÖZET

SİNÜZOİDAL SOĞUTMA KANALLARINDAKİ SOĞUTUCU SİRKÜLASYONU İÇİN POMPA GÜCÜ MİNİMİZASYONUNUN SAYISAL İNCELENMESİ

Elektronik birimler yaptıkları işlem hacmi arttıkça daha fazla güç tüketmektedirler. Buna bağlı olarak sıcaklıkları artmakta ve yeterli şekilde soğutulamadıklarında ise elektronik elemanlar güvenli çalışma sıcaklığını aşarak çalışamaz duruma gelmektedir. Elektronik sektöründeki ilerlemeler ısı transferindeki bu dar boğazları aşabildikleri sürece daha güçlü seviyelere gelmektedir. Soğutma sistemleride bir elektriksel güç harcamakta ve bu enerjinin minimize edilmesi gerekmektedir. Bu tezde bir elektronik elemanı soğutmak için harcanan enerjinin minimizasyon çalışması gerçekleştirlmiştir.

Bu çalışmada, dikdörtgen kesitli sinüs dalgalı kanallardaki ısı transferi sayısal yöntemlerle incelenmiş ve ısı transferindeki iyileştirmeler düz bir kanal geometrisi referans alınarak değerlendirilmiştir. Kanal geometrisindeki farklı genlik ve dalga boyları için pompa gücü ve yüzey sıcaklığındaki iyileştirmeler üzerinde durulmuştur. Kanal içerisindeki akış Re sayısı 7 ile 368 arasında, laminer ve zamandan bağımsız olarak kabul edilmiştir. Soğuk plaka üzerindeki elektronik modülden yayılan ısı akısı sabit alınmıştır. Elektronik modül üzerindeki kritik eleman sıcaklığı gözlemlenerek termal performans ve kanal içerisindeki basınç düşümü hesaplarından yararlanılarak pompa gücü hesaplanmıştır. Sinüs dalgalı kanalın düz kanala göre soğuk plakayı nasıl etkilediğini görebilmek için bazı boyutsuz performans sayıları tanımlanmıştır ve değerlendirmeler bu boyutsuz sayılar ışığında yürütülmüştür.

Genel olarak sinus dalgalı kanalın ısı transfer performansını arttırdığı gözlemlenmiştir. Dalga genliği ısı transferini olumlu etkilerken, pompa gücünü olumsuz yönde etkilemiştir. Isı transferi performansının gelişiminde dalga boyunun etkisinin dalga genliği kadar önemli olmadığı görülmüştür. Fakat büyüyen dalga boyuyla birlikte pompa gücünün azaldığı gözlemlenmiştir.

TABLE OF CONTENTS

LIST OF FIGURES viii

LIST OF TABLES xi

LIST OF SYMBOLS xii

CHAPTER 1. INTRODUCTION 1

1.1. Thesis Objective 6

CHAPTER 2. LITERATURE SURVEY 7

CHAPTER 3. NUMERICAL ANALYSIS 12

3.1. Introduction to Computational Fluid Dynamics 12

3.2. Description of the Problem and Geometry 14

3.2.1. Thermal Resistance and Junction Temperature 16

3.2.2. Properties of Electronic Devices and Calculation of Temperature Limit 18

3.3. Channel Geometries and Specifications 21

3.3.1. Straight Channel Geometry 21

3.3.2. Wavy Channel Geometry 23

3.4. Material Properties 26

3.4.1. Thermo-physical Properties of Aluminum 26

3.4.2. Thermo-physical Properties of Working Fluid 26

3.5. Boundary Conditions 27

3.5.1. Inlet Boundary Condition 27

3.5.2. Outlet Boundary Condition 28

3.5.3. Wall Boundary Condition 29

3.6. Governing Equations 30

3.7. Overview of Numerical Solution 32

3.8. Mesh Generation and Computational Details 34

3.8.1. Mesh Generation 34
3.8.2. Computational Details 38

CHAPTER 4. RESULTS AND DISCUSSION 39
4.1. Results of the Straight Channel Geometry 39
4.2. Results of the Sinusoidal Wavy Channel Geometry 40
4.2.1. Effect of Wave Amplitude 43
4.2.2. Effect of Wavelength 57

CHAPTER 5. CONCLUSION 68

REFERENCES 70

LIST OF FIGURES

Figure **Page**

Figure 1.1. Heat transfer mechanisms 2
Figure 1.2. Various cooling applications a) indirect cooling b) internal direct cooling (Source: Cengel 2007) 3
Figure 1.3. Cooling of power transistors on a cold plate 3
Figure 1.4. A cold plate geometry 4
Figure 1.5. Various channel geometries a) A straight channel b) A sinusoidal wavy channel c) A V corrugated wavy channel 5
Figure 1.6. A cold plate using in the power electronics cooling 5
Figure 2.1. Comparison of experimental and numerical results for the pressure drop with different Re numbers (Source: Qu and Mudawar 2006) 8
Figure 2.2. Variation of Nusselt number with Reynoulds number for different amplitude wavelength ratio (Source: Wang and Chen 2002) 9
Figure 2.3.Variation in average Nusselt number and pressure drop with amplitude (Source: Gong et al. 2011) 9
Figure 3.1. View of electronic module and cold plate 14
Figure 3.2. The geometric details of the electronic module and positions of the electronic devices 15
Figure 3.3. The geometric details of the cold plate 16
Figure 3.4. Thermal resistance in the electronic assembly 17
Figure 3.5. Junction temperature with failure rate 18
Figure 3.6. Temperature points for T_{case} 19
Figure 3.7. The straight channel geometry 22
Figure 3.8. Geometry of wavy channel in cold plate 23
Figure 3.9. Wavy passage configurations for different phase shifting angle (a) φ=0°, (b) φ=90°, (c) φ=180° (Source: Rush et al. 1999) 24
Figure 3.10. General view of wavy channel geometries 25
Figure 3.11. Thermo-physical properties of 50% ethylene-glycol water mixing 27
Figure 3.12. Inlet boundary condition surface in the model 28
Figure 3.13. Outlet boundary condition surface in the model 29
Figure 3.14. Wall boundary conditions in the model 30

Figure 3.15. Overview of the solution method 33
Figure 3.16. Mesh generation in the model (A-X sight, B-Z sight and C-Ysight) 35
Figure 3.17. Mesh independence analyses for the straight channel geometry at Re=368 36
Figure 3.18. Mesh independence analyses for sinusoidal wavy channel geometry A=40 mm λ=120 mm at Re=368 37
Figure 4.1. Variation in T_{case} with Re number 40
Figure 4.2. Variation in W_{pump} with Re number 40
Figure 4.3. Performed the sinusoidal wavy channel geometries in the study 41
Figure 4.4. Variation in TR with Re for λ=40 mm 43
Figure 4.5. Variation in TR with Re for λ=60 mm 44
Figure 4.6. Variation in TR with Re for λ=120 mm 44
Figure 4.7. Variation in TR with Re for λ=180 mm 45
Figure 4.8. Comparison of temperature contours for different wave amplitudes a) A=5mm λ=60mm b) A=40mm λ=60mm 46
Figure 4.9. Comparison of temperature contours for different wave amplitudes a) A=5mm λ=120mm b) A=40mm λ=120mm 46
Figure 4.10. Variation of heat transfer coefficient contour line for different wave amplitudes at Re=368 a) A=5mm λ=60mm b) A=40mm λ=60mm 47
Figure 4.11. Variation in WR with Re for λ=40mm 49
Figure 4.12. Variation in WR with Re for λ=60mm 49
Figure 4.13. Variation in WR with Re for λ=120mm 50
Figure 4.14. Variation in WR with Re for λ=180mm 50
Figure 4.15. Pressure distribution for different wave amplitudes at Re=368 51
Figure 4.16. Pressure distribution for different wave amplitudes at Re=368 51
Figure 4.17. Velocity vector for A=5mm λ=60mm at Re=368 53
Figure 4.18. Velocity vector for A=40mm λ=60mm at Re=368 54
Figure 4.19. Variation in PF with Re for λ=40mm 55
Figure 4.20. Variation in PF with Re for λ=60mm 55
Figure 4.21. Variation in PF with Re for λ=120mm 56
Figure 4.22. Variation in PF with Re for λ=180mm 56
Figure 4.23. Variation in TR with Re for A=5mm 57
Figure 4.24. Variation in TR with Re for A=10mm 58

Figure 4.25. Variation in TR with Re for A=20mm 58
Figure 4.26. Variation in TR with Re for A=40mm 59
Figure 4.27. Comparison of temperature contours for different wavelengths
a) A=10mm λ=40mm b) A=10mm λ=180mm.....60
Figure 4.28. Comparison of temperature contours for different wavelengths
a) A=20mm λ=40mm b) A=20mm λ=180mm.....60
Figure 4.29. Variation of heat transfer coefficient contour line for different
wavelengths a) A=10mm λ=40mm b) A=10mm λ=180mm.....61
Figure 4.30. Variation in WR with Re for A=5mm 61
Figure 4.31. Variation in WR with Re for A=10mm 62
Figure 4.32. Variation in WR with Re for A=20mm 62
Figure 4.33. Variation in WR with Re for A=40mm 63
Figure 4.34. Pressure distribution for different wavelengths at Re=368
a) A=10mm λ=40mm b) A=10mm λ=180mm.....63
Figure 4.35. Pressure distribution for different wavelengths at Re=368
a) A=20mm λ=40mm b) A=20mm λ=180mm.....64
Figure 4.36. Velocity vector for A=10mm λ=40mm at Re=368 65
Figure 4.37. Velocity vector for A=10mm λ=180mm at Re=368 65
Figure 4.38. Variation in PF with Re for A=5mm 66
Figure 4.39. Variation in PF with Re for A=10mm 66
Figure 4.40. Variation in PF with Re for A=20mm 67
Figure 4.41. Variation in PF with Re for A=40mm 67

LIST OF TABLES

Table **Page**

Table 3.1. Properties of electronic devices 18

Table 3.2. $T_{case\max}$ of electronic devices 21

Table 3.3. Thermo-physical properties of 6061-T6 Aluminum 26

LIST OF SYMBOLS

ED	Electronic device	
PF	Performance factor	
TR	Temperature ratio	
WL	Wavelength	
WR	Pump power ratio	
Al	Aluminum	
a	Height of channel	mm
b	Width of channel	mm
A	Wave amplitude	mm
A_c	Cross sectional area of channel	m^2
D_h	Hydraulic diameter	m
L	Hydrodynamic entry length	m
P	The wetted perimeter	m
q	Power dissipation	W
P_{inlet}	The average pressure of the inlet surface	bar
P_{outlet}	The average pressure of outlet surface	bar
ΔP	Pressure drop	bar
Re	Reynolds number	
$T_{case\max}$	Reliable operating temperature	°C
T_{case}	The average temperature of contact surface of critic ED and electronic module	°C
T_j	Junction temperature	°C
T_{ref}	The average surface temperature of the case surface for the straight channel	°C
V_{mean}	Average velocity	m/s
W_{pump}	Pump power	mW
$W_{pumpref}$	Pump power of the reference channel	mW
ρ	Density	kg/m^3
μ	Dynamic viscosity	kg/m.s

$\dot{\vee}$	Volumetric flow rate	m^3/s
λ	Wavelength	mm
φ	Phase shifting angle	º
θ_{jc}	Junction to case thermal resistance	ºC/W
θ_{cs}	Case to heat sink thermal resistance	ºC/W
θ_{sa}	Heat sink to ambient thermal resistance	ºC/W
θ_{tot}	Total thermal resistance	ºC/W
Gr	Grashof number	
g	Acceleration of gravity	m/s^2
β	Expansion coefficient of fluid	1/K
ν	Kinematic viscosity of fluid	m^2/s

CHAPTER 1

INTRODUCTION

Electric devices and equipment take place in widespread area in our daily life. It is possible to encounter high powered electronic devices in many applications such as transmitters, lasers, power drivers, medical equipment, high performance computers and aerospace flight electronics.

The field of electronic has begun since 1880s, when the vacuum diode was invented by Thomas Edison. The vacuum tube encouraged great contributions to the development of radio, TV, radar and digital computer. Since the development of the first electronic digital computers in the 1940s, the effective cooling of electronic devices plays very important role to ensure reliable operation of computers. The Electrical Numerical Integrator and Computer (ENIAC) was launched in 1946 which had 18000 vacuum tubes. Industrial cooling fans were used to remove the 140kW heat dissipated from its tubes (Bergles, 1986).

The solid state transistor was invented by Bardeen, Brattain and Shockley in 1947. As a replacement for vacuum tubes, the transistor generated less heat and was much more reliable and had lower production costs. Another turning point in the field of electronic was appeared in 1959 with the production of the Integrated Circuits (IC), which contains several components such as diodes, transistors and capacitors. The number of components in the integration was between 50 and 1000 per chip in 1960s which increased until 100000 components per chip at the end of 1970. In the 1980s, approximately 10 million components per chip were used to generate very large scale integration (VLSI). Nowadays, a chip 3cmX3cm in size consists of several million components.

When an electrical current is conducted through a semiconductor or other electronic devices, a portion of its power is lost and therefore dissipated as heat. Moreover, this heat generation results in increase of temperature in the component if not removed, until the component is destroyed. Therefore, cooling of an high power electronic device is a necessity for it to function properly. The maximum operating

temperature specified by the manufacturer is an important parameter in terms of safety and reliability of the all systems.

The cooling system must be designed considering the operating conditions. Military operating conditions are a striking example for this since, the electronic system is exposed to high ambient temperatures, high degree of vibration, solar heating and corrosive conditions are some of these demanding conditions. Cooling systems in principle can be divided two main categories as direct and indirect cooling. Electronics are in direct contact with the coolant in direct cooling and therefore the heat generated in the components is transferred directly to the fluids. All the air cooled systems can be considered to be direct cooling systems. On the other hand, liquid cooling is usually done as indirect cooling in which electronics and coolant are separated by a sealed surface, since coolant are not usually dielectric. The heat is generated in the component and transferred to a medium such as a cold plate where liquid is sealed in, before it is carried away by the circulating liquid. In Figure 1.1 shows common heat transfer mechanisms for direct and indirect cooling, and signify effectiveness of the different cooling techniques. In Figure 1.2 shows a typical components of direct and indirect cooling systems.

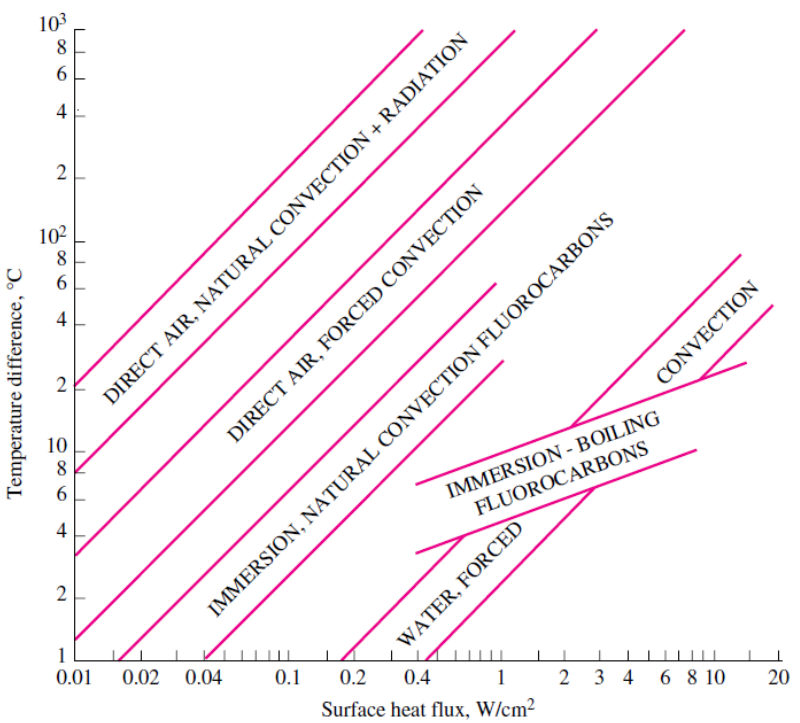

Figure 1.1. Heat transfer mechanisms
(Source: Kraus and Bar-Cohen 1983)

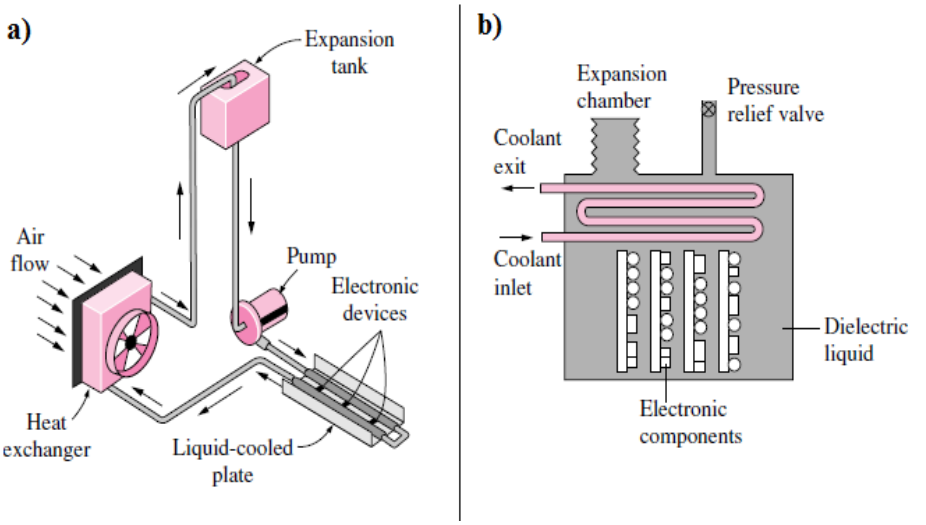

Figure 1.2. Various cooling applications a) indirect cooling b) internal direct cooling (Source: Cengel 2007)

The efforts have been made to produce more efficient heat exchangers by employing various methods of heat transfer enhancement and minimizing the pressure drop. Savings in materials and energy are so important factor for the industries because in these days the cost of energy consumption in the applications is rapidly increasing. Therefore, the any energy improvement of the cooling system is crucial for especially in automotive, aerospace and electronics industries in which a worldwide mass consumption exists.

In direct liquid cooling is the main topic of this thesis and in a typical application it works as following; the heat producing electronic components are mounted on a metal plate made of a highly conducting material such as copper or aluminum. The heat sinks or cold plates of an electronic system are usually cooled by water or water mixing by passing it through channels made for this purpose or through tubes attached to the cold plate. High heat removal rates can be achieved by circulating water through these channels or tubes. A cold plate application is illustrated in Figure 1.3.

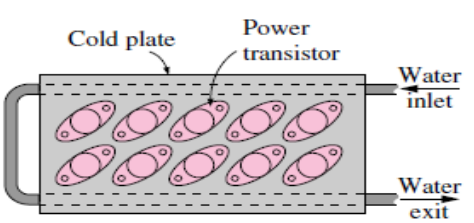

Figure 1.3. Cooling of power transistors on a cold plate (Source: Cengel 2007)

Another cold plate application with electronic modules mounted on it is illustrated in Figure 1.4-a. The channel geometry and position in the cold plate can be seen in Figure 1.4-b.

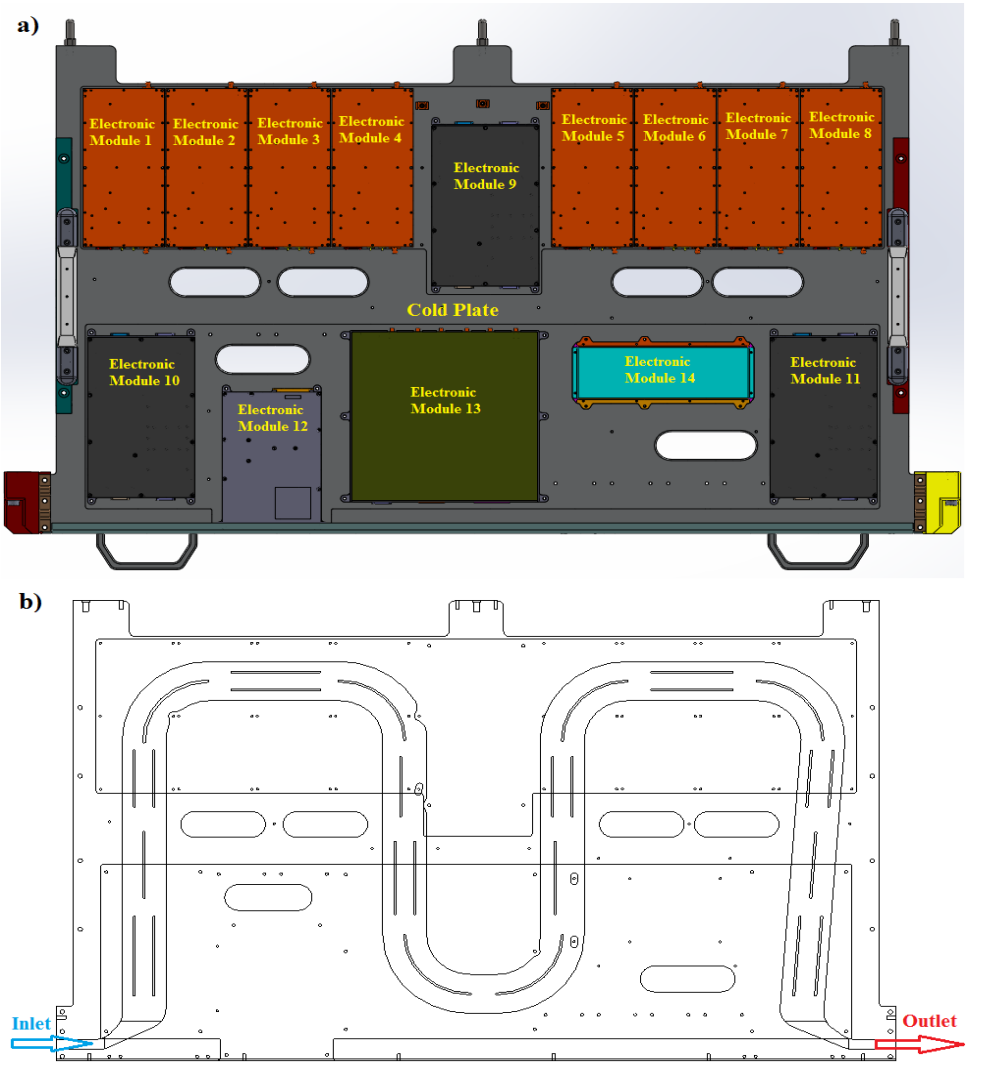

Figure 1.4. A cold plate geometry

Heat load and pressure drop are crucial two factors which must be considered when a cold plate heat exchanger is designed. The different channel geometries are used in the cold plate in order to achieve desired heat transfer such as a straight channel or, various wavy channels types (V type, sinusoidal, rectangular, etc.), as shown some of them in Figure 1.5.

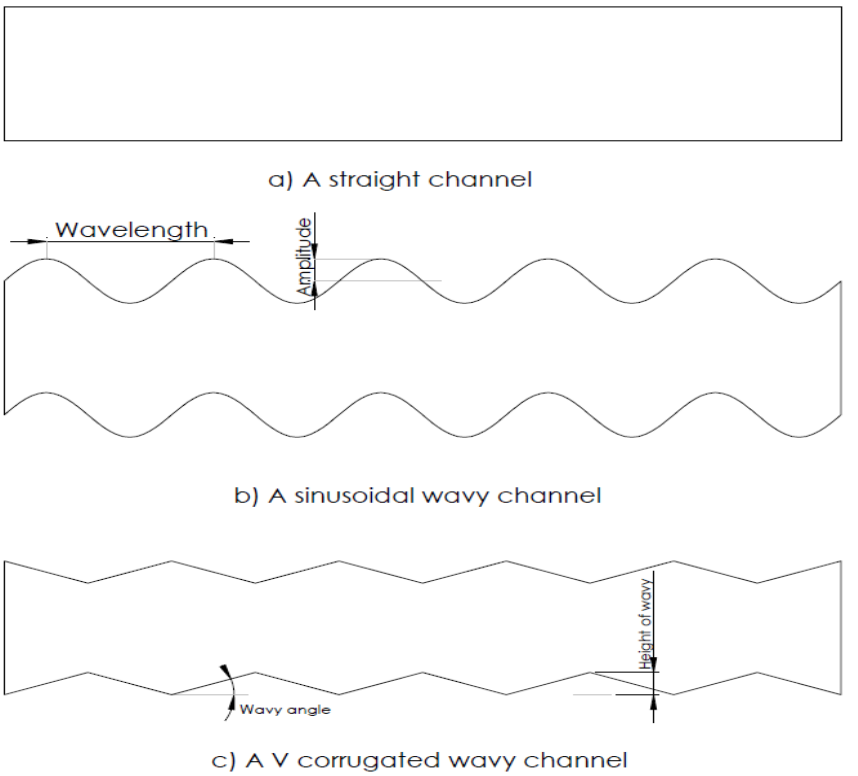

Figure 1.5. Various channel geometries a) A straight channel b) A sinusoidal wavy channel c) A V corrugated wavy channel

Another application of specific cold plate, which in this case a vacuum brazed aluminum, for power electronics cooling in a military application is shown in Figure 1.6. Mounting locations of the electronic components and liquid inlet/outlet ports can be seen in this figure.

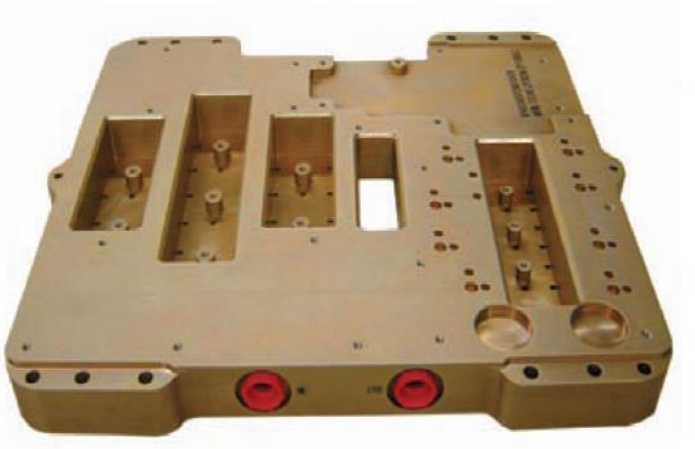

Figure 1.6. A cold plate using in the power electronics cooling (Source: Lytron Inc.)

1.1. Thesis Objective

The primary goal of this thesis is to investigate enhancement of heat transfer as much as possible while minimizing pressure drop for the different sinusoidal wavy channel geometries in a cold plate. A straight channel geometry is determined as a reference model and all sinusoidal wavy channel geometries are compared with it in order to determine whether the heat transfer and pressure drop are improved or not.

A numerical study of three dimensional laminar fluid flow and heat transfer in sinusoidal wavy channel is performed by varying the wave amplitude, wavelength for different Re numbers between 7 and 368 with steady state condition. A constant heat fluxes from the dissipating electronic devices and cross sectional area of the channel ($2x60mm^2$) are used for all channel geometries in the model.

A performance factor (PF) is defined to evaluate the overall performance (the enhancement in both heat transfer and pressure drop) of the model.

CHAPTER 2

LITERATURE SURVEY

Numerous studies have been performed about heat transfer and/or pressure drop (or pump power) in corrugated or wavy channel for last few decades. The heat transfer performance and pressure drop can be affected by many parameters such as wave geometry, wave amplitude, wave length, flow rate, and flow conditions. A lot of applications of wavy channels exist in the literature. The aim of this chapter is to summarize the literature in the scope of this work.

The pressure drop and heat transfer characteristics of a straight micro channel were studied experimentally and numerically by Qu and Mudawar (2002). The model is performed at the two different constant heat flux levels, the range of Reynolds number is between 139 and 1672. They showed that both the heat sink temperature and water outlet temperature decrease with higher Reynolds numbers. This effect is a profitable factor in terms of heat transfer but which increases pressure drop. They obtained agreeing results compared with numerical predictions and experimental data. This deduction gives a confidence that the numerical approaches can be used for practical cooling applications.

Qu and Mudavar (2006) observed flow development and pressure drop using experimental and computational techniques for adiabatic single-phase water flow. They used a single rectangular micro channel 222μm wide, 694 μm deep and 12cm long. Their assumptions were steady flow, incompressible fluid, laminar flow and constant solid and fluid properties. The SIMPLE algorithm was used to solve the resulting system of algebraic equations in primitive variables and the Gauss-Seidel iterative technique was employed in the solution process. The pressure drop measurements were reported at Reynolds numbers of 196, 1021, 1895, and 2215. Once experimental and numeric results were compared, the numeric predictions denoted excellent agreement with experimental data. The Figure 2.1 shows comparison of experimental and numerical results for pressure drop at different Reynolds numbers.

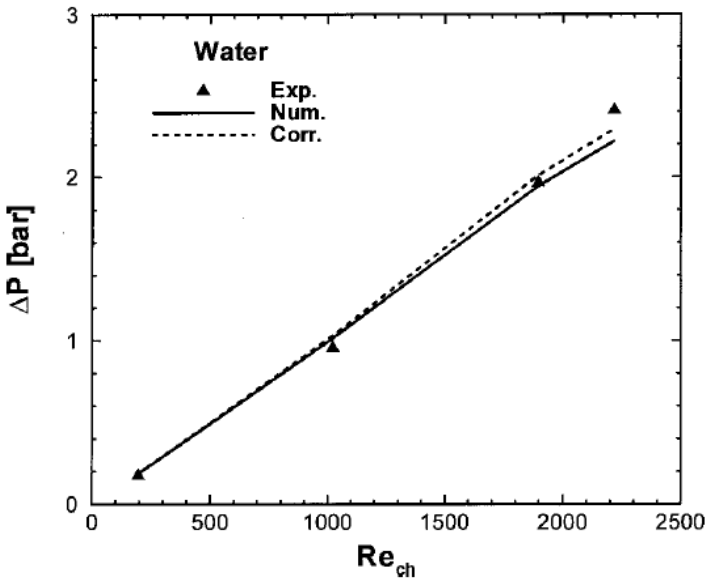

Figure 2.1. Comparison of experimental and numerical results for the pressure drop with different Re numbers (Source: Qu and Mudawar 2006)

The heat transfer performance of a corrugated channel was optimized numerically and which compared to a smooth wall duck under laminar flow condition by Fabbri (2000). In this study, some constraints were carried out to model such as channel size and the wall volume at the low Re numbers. The heat performance can be increased at this condition but especially at higher Re numbers, optimum corrugated wall profile provides approximately 30% heat transfer enhancement. As a consequence, a corrugated wall always exhibits better heat transfer performance with respect to a smooth wall.

Forced convection for a wavy wall channel was investigated numerically in order to detect flow and heat transfer characteristics by Wang and Chen (2002). The channel geometry was studied with varied wavy amplitude-wavelength ratios and Re numbers in the range of 100 and 500. The amplitude-wavelength ratio contributes significant heat transfer enhancement compared to a straight channel. Moreover, especially at higher Re numbers, the amplitude-wavelength ratio is very effective in terms of heat transfer but this effect is not important at low Re numbers. Variation of average Nusselt number with Reynolds number for different amplitude wavelength ratios is shown in Figure 2.2.

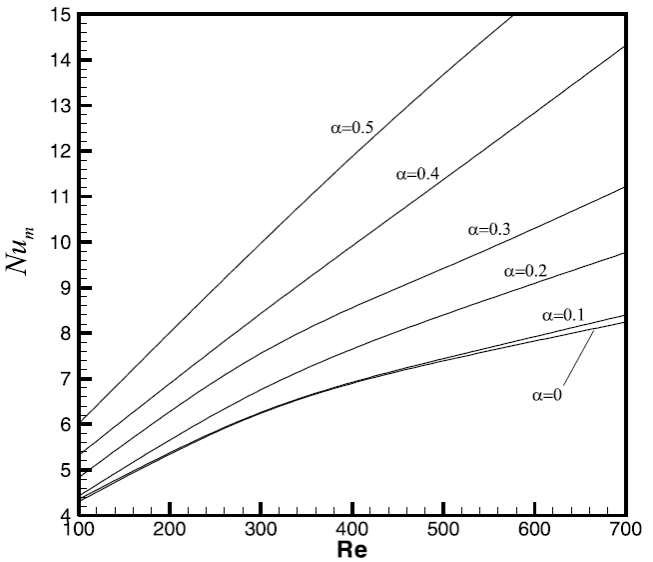

Figure 2.2. Variation of Nusselt number with Reynoulds number for different amplitude wavelength ratio (Source: Wang and Chen 2002)

Gong et al (2011) investigated fluid flow and heat transfer characteristics in wavy micro channels which were performed at different wavy amplitudes, wavelengths and aspect ratio at the various Re numbers. They compared thermal performance and flow characteristics of wavy and straight channels at a constant heat flux of 47 W/cm^2. They reported that the Nu and Δp were increased with amplitude and Re number. This effect is shown in Figure 2.3. When the wavelength was decreased, thermal performance was greatly influenced but it was not a crucial factor compared with amplitude.

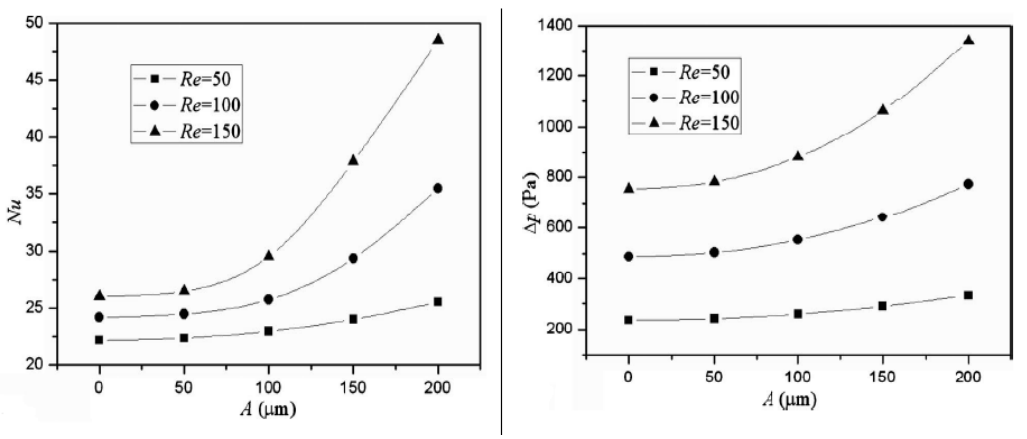

Figure 2.3.Variation in average Nusselt number and pressure drop with amplitude (Source: Gong et al. 2011)

Rush and Jacobi (1999) studied on local heat transfer and flow behavior for laminar and transitional flows in a sinusoidal wavy channels. In their study, the walls of a channel are from 12 to 14 wavelengths long (λ), and the channel was investigated at different wave amplitudes (A), phase angles (φ). They used the some dimensionless variables to identify the flow in the sinusoidal wavy channels, which are phase shift (φ), relative amplitude (A/Hmin), relative wavelength (λ/Hmin) and Reynolds number but the value of Reynolds number is always smaller than 1000 in the experiments. Phase shift plays an important role in the heat transfer enhancement. They observed that the location of the onset of mixing in the channel moves near the entrance of the channel, when the flow is steady state and φ =180^{o}. This mixing positively affects the thermal development. The same observations were repeated for the φ =0^{o} and φ =90^{o} but the location of the onset of mixing is not closer than φ =180^{o}. They revealed that the relative amplitude more effective than relative wavelength because which leads to the onset of mixing at the lower Reynolds numbers. Additionally, if the mixing does not occur in the fully developed flow at the low Re numbers, the heat transfer characteristic of wavy channel is approximately the same as a straight channel.

Heat transfer performance and pressure drop were investigated numerically both using steady and unsteady regime for straight channel, sinusoidal channel and arc-shaped channel by Niceno and Nobile (2001). Their results showed that unsteady regime was seen at Re=200. At this regime, heat transfer enhancement is more effective compared to steady regime for sinusoidal wavy channel. At the same time, pressure drop is higher than steady regime. Moreover, heat transfer augmentation is better in the sinusoidal channel for the unsteady regime compared to straight channel.

Heat transfer and flow characteristic in sinusoidal channels were performed numerically by Metwally and Manglik (2004). The channels were investigated with different amplitudes, wavelengths, and Re numbers between 10 and 1000. Their results indicate that the amplitude and Re number do not affect heat transfer enhancement significantly, especially in the steady flow but when the flow displays unsteady flow structure which seen approximately at Re=300, the enhancement of heat transfer is very effective. They compared it to straight channel and found that the heat transfer enhancement is 34 folds but friction factor is 18 times higher.

Nishimura et al (1984) investigated flow characteristics in a sinusoidal wavy channel by numerically and experimentally. The flow was observed in the Re number

range of 100 to 1000. They reported that, the wavy channel displays laminar flow characteristic at Re number less than 350 at which the flow begins unsteady regime.

Hossain and Islam (2004) studied on fully developed unsteady flow and heat transfer in a sinusoidal wavy channel by using two dimensional Navier-Stokes and energy equations numerically. They observed that increasing Re number leads unsteady flow which causes enhancement of heat transfer and pressure drop. For the sinusoidal wavy channel, the flow starts to show unsteady characterization at Re=205. They observed that increment of amplitude leads more fluctuations in the flow and more pressure drop in the channel. Therefore, the flow becomes unsteady at a lower Reynolds number with increasing amplitude. In addition, they performed various wavelengths but which has a minimal effect on the flow behavior.

The heat transfer performance and pressure drop were investigated in the V-type corrugated channel under constant heat flux by Naphon (2007). The different corrugated angles and Re numbers in the range of 2000-9000 were observed experimentally. Flow in this Re number range is known to be turbulent. The experiments showed that the corrugations results in heat transfer enhancement. The wave angle increases heat transfer performance but the pressure drop increases slowly.

CHAPTER 3

NUMERICAL ANALYSIS

3.1. Introduction to Computational Fluid Dynamics

Computational Fluid Dynamics (CFD) involves in numerical solutions of governing equations of fluid motion which are partial differential equations of conservation of mass, momentum and energy. It shortly means that prediction of fluid flow and heat transfer characteristics by using computationally numeric methods. Some of the application areas of CFD are;

- Aerospace: Design of aerodynamics of aircrafts, wing and rocket design
- Chemical Engineering: Multiphase systems, mixing
- Construction: HVAC design, ventilation modeling
- Electric and Electronic: Cooling of electronic devices
- Healthcare: Cardiovascular, filtration for pollution
- Marine: Ship Design, blade geometry
- Turbomachinery: Design of blade geometry, compressor and turbochargers.

CFD has been started to be used firstly in 1960's by the aerospace industry. CFD techniques have been embedded in the design, R&D and manufacturing of aircraft and jet engines but especially it was started to be broadly used by different industries in 1970's. These applications showed that CFD has a lot of advantages for industries in the design and manufacturing products. Therefore, CFD became a significant part of various industries and academic studies.

If CFD and experimental applications are compared, some crucial profits of CFD can be observed. These are listed in below.

- The significant time and cost saving for new products.
- Getting information about complexity and impossible situations in real cases.
- The investigation of risky and dangerous cycles such as nuclear studies.

CFD codes are configured around the numerical algorithms which solve fluid flow and heat transfer problems. The problem could be easily defined, solved and evaluated by use of three steps which are

Pre-Processor: Pre-processing section comprises of establishing input elements of flow problems, which prepares the model for another section in order to solve. There are some steps, which are completed by the analyzer (Versteeg and Malalasekera 1995);

- Definition of the geometry of the region of interest: the computational domain.
- Grid generation-the sub division of the domain into a number of smaller, non-overlapping sub-domains: a grid (or mesh) of cells (or control volumes or elements).
- Selection of the physical and chemical phenomena that need to be modeled.
- Definition of fluid properties.
- Specification of appropriate boundary conditions at cells which coincide with or touch the domain.

The number of cells affects significantly the accuracy of a CFD solution. If the grid is fine, the number of cells used is high but this is better for solution accuracy. On the other hand, it increases solution time and necessary computer resorces. Therefore, when the model is prepared for solving, the optimal meshes must be used so that the total cost of the solution can be kept down.

Solver: The different streams of numerical solution techniques exist which are finite difference, finite element and spectral methods. The finite volume method was improved as a special formulation of finite difference schemes. The numerical methods comprise of the following steps (Versteeg and Malalasekera 1995):

- Formal integration of the governing equations of fluid flow over all the control volumes of the solution domain.
- Discretization involves the substitution of a variety of finite-difference-type approximations for the terms in the integrated equation representing flow processes such as convection, diffusion and sources. This converts the integral equations into a system of algebraic equations.

Post-Processor: Post-processing section provides to evaluate the results of solution. This section presents some opportunities about the problem (Versteeg and Malalasekera 1995):

- Domain geometry and grid display
- Vector plots

- Line and shaded contour plots
- 2D and 3D surface plots
- Particle tracking
- View manipulation (translation, rotation, scaling, etc.)
- Color postscript output

3.2. Description of the Problem and Geometry

In this study, an electronic cooling module utilizing a cold plate is investigated for the limited temperature. The performance of the system is observed with computational calculations in terms of heat transfer and pressure drop. The results of the calculation are examined to find out an optimal geometry in which temperature limits are not exceeded and the pump power is minimized. During the computational analyses, the different channel geometries and volumetric flow rates are applied to the cold plate such as a straight channel or a sinusoidal channel. Figure 3.1 shows general view of the electronic module and the cold plate investigated in this thesis.

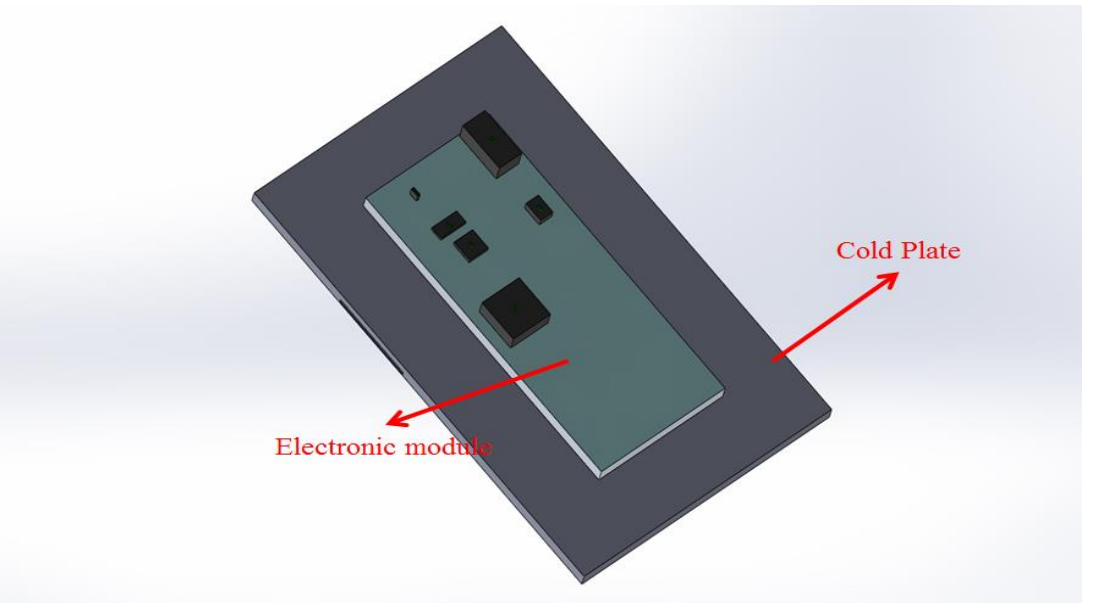

Figure 3.1. View of electronic module and cold plate

The electronic module consists of an aluminum block and six electronic devices. When the electronic devices start to work, they generate considerable waste heat. Therefore, this waste heat must be removed away from the electronic devices and the

devices must be hold below a safe temperature. The waste heat is taken from electronic devices first by the aluminum block of electronic module and transferred to the cold plate. This heat is taken from the cold plate by the circulating fluid. 50 % ethylene glycol and water mixing is used as a coolant fluid because of its wide use in practice.

The electronic module's block and the cold plate are made of 6061-T6 alloy of aluminum. The geometric details of the electronic module and cold plate are denoted in Figure 3.2 and Figure 3.3.

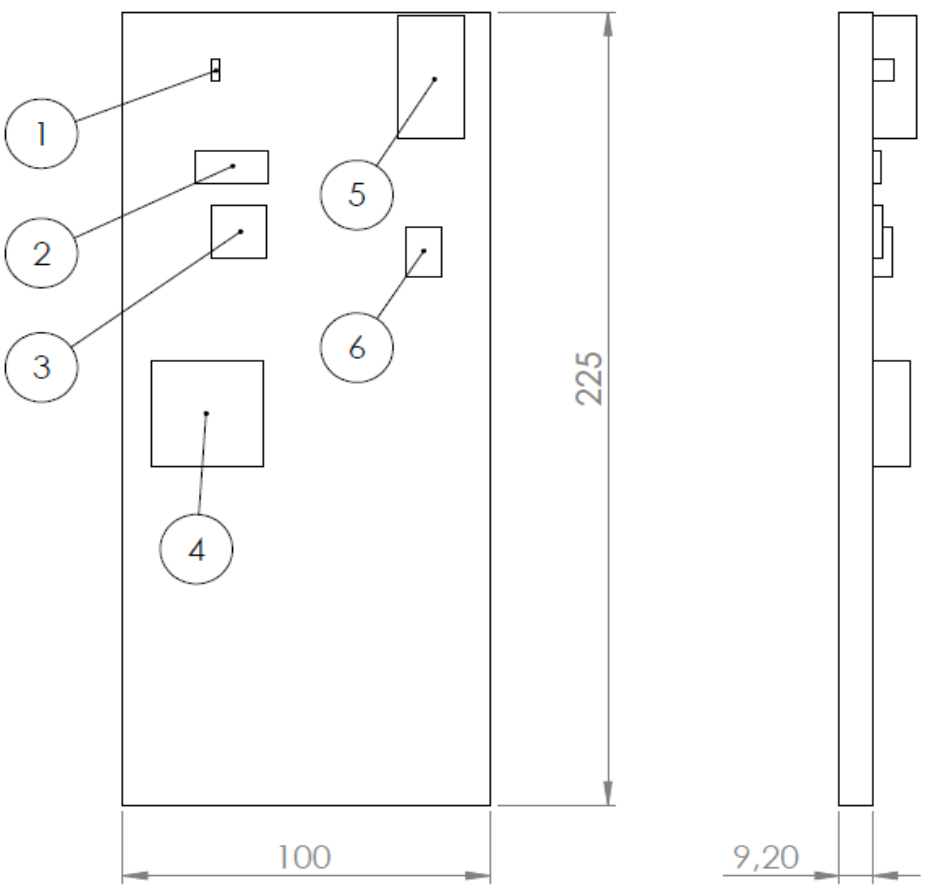

Figure 3.2. The geometric details of the electronic module and positions of the electronic devices

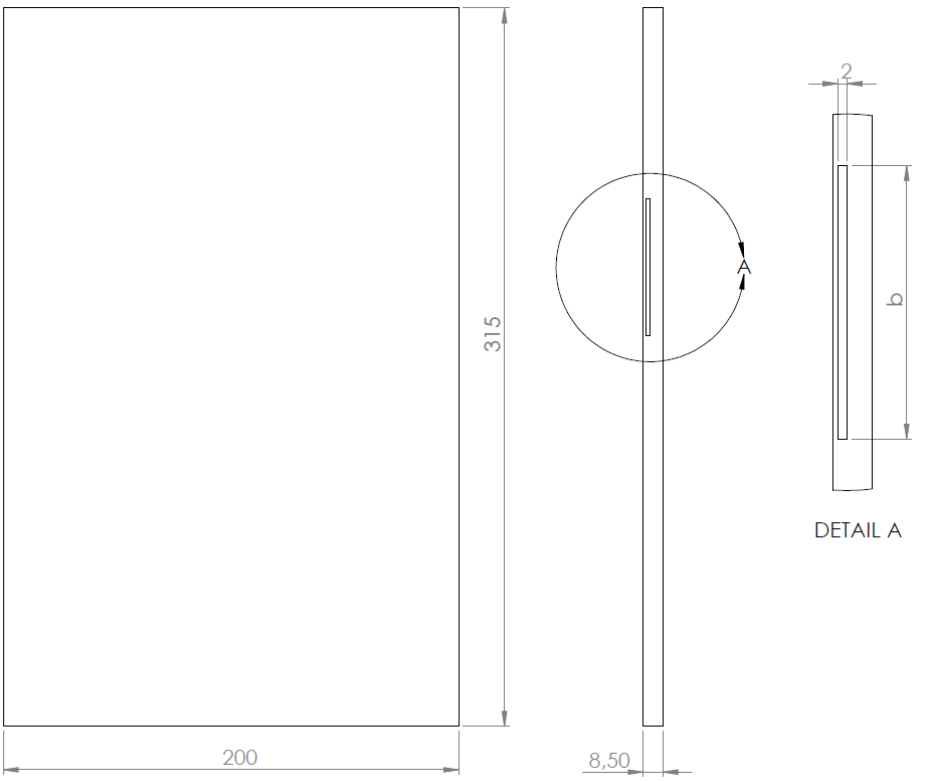

Figure 3.3. The geometric details of the cold plate

The Figure 3.3 shows the dimensions of the cold plate and the coolant channel. The height of the channel has a constant value 2 mm. The width of the channel is constant and 60 mm for all geometries.

3.2.1. Thermal Resistance and Junction Temperature

Thermal resistance, θ, is defined as a measure of material's ability to resist heat transfer. Thermal resistance between two different temperatures is an analogy to an electrical resistor between a potential difference. Some of the important thermal resistances used in this. These are i) θ_{jc} which occurs between the semiconductor junction (j) and the junction's external case (c), ii) θ_{cs} which is a resistance between the case and the heat sink interface surface and iii) θ_{sa} which represent a thermal resistance between the heat sink interface surface and ambient. These are showed schematically in Figure 3.4. Thermal resistance varies by many factors such as package type and size, heat sink material and geometry, die size, circuit power, etc. Unit of thermal resistance is ºC/W.

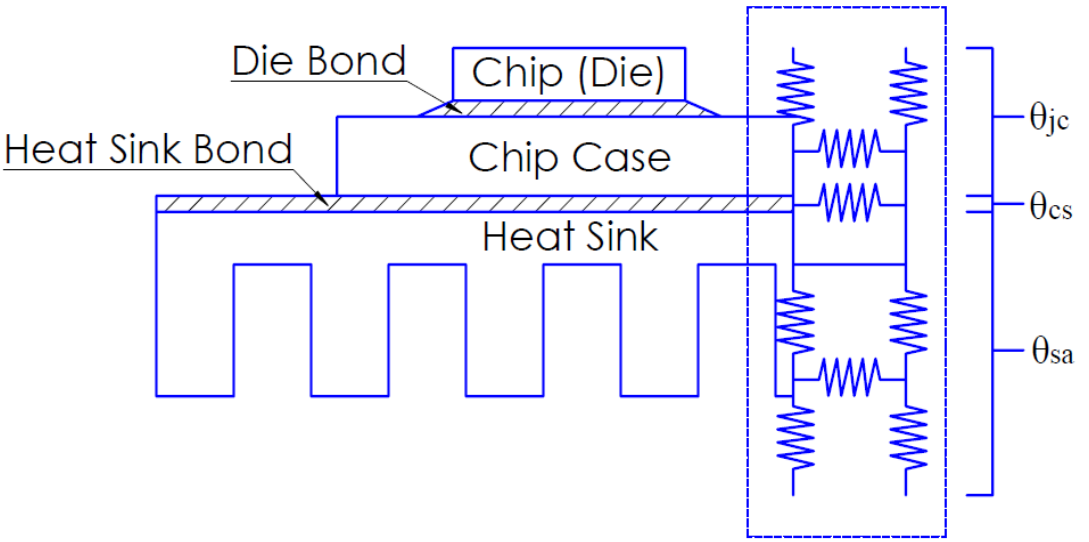

Figure 3.4. Thermal resistance in the electronic assembly

Total thermal resistance which is defined between electronic devices center (junction) and ambient, θ_{tot}, is represented by the Eq. 3.1 as below.

$$\theta_{tot} = \theta_{jc} + \theta_{cs} + \theta_{sa} \qquad 3.1$$

where θ_{jc}, θ_{cs} and θ_{sa} are defined above.

Junction temperature is usually used in semiconductor devices for die or device temperature. Junction temperature is a criterion for determining of the operating life of devices. Therefore, it affects heat transfer and thermal design in the system. The operating life of devices decreases with increased junction temperature so junction temperature must be held below a determined limit temperature by the semiconductor manufacturers. Figure 3.5 shows junction temperature versus failure rate (Ralph Remsburg 2001).

The determining junction temperature is very important criterion for effective thermal designs. Equation 3.2 is used for calculation of junction temperature.

$$T_j = T_{case\max} + \theta_{jc} q \qquad 3.2$$

where T_j is junction temperature, $T_{case\max}$ is reliable operating temperature, and q power dissipation (W).

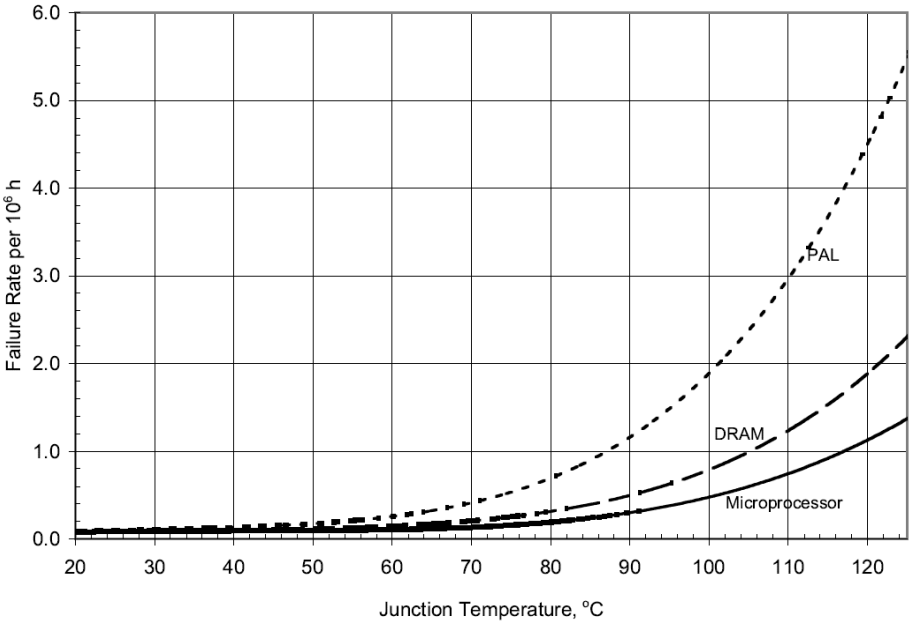

Figure 3.5. Junction temperature with failure rate
(Source: Ralph Remsburg 2001)

3.2.2. Properties of Electronic Devices and Calculation of Temperature Limit

The thermal properties of electronic devices marks the limits of analyses, therefore, it is very important to prepare the CFD model for reliable solutions. In this study, six different electronic devices, which are shown in Figure 3.2, and properties are listed in Table 3.1 are used.

Table 3.1. Properties of electronic devices

Component	$T_{junction}$ °C	θ_{jc} °C/W	Power Dissipation W
ED 1	130	64	0.65
ED 2	150	15	1.4
ED 3	225	2.5	58
ED 4	175	7.5	12
ED 5	161	56	1
ED 6	175	0.4	0.1

The limits of the temperature are determined by the case temperature of electronic devices in the study. T_{case} is a value of the temperature where taken from the

case of chip which can be seen in Figure 3.4. Figure 3.6 shows that where the T_{case} is measured on the electronic module's surface in the analyses. When the numerical calculations are converged, corner point temperatures of the case are taken from electronic module surface and their arithmetic mean gives T_{case} as in Equation 3.3

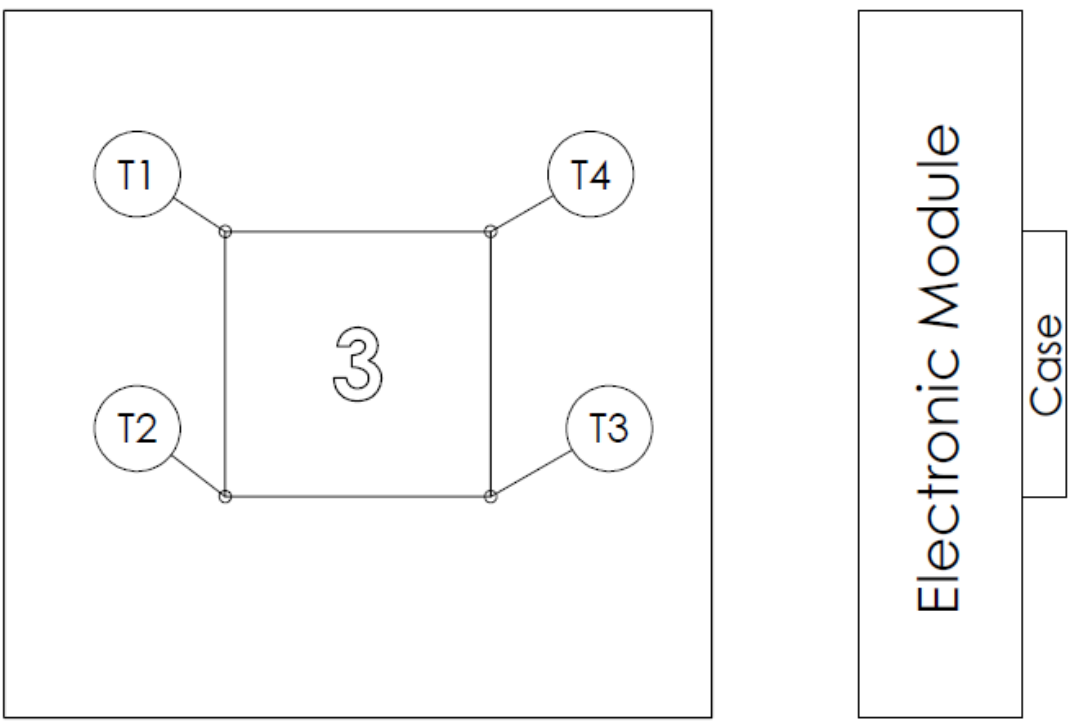

Figure 3.6. Temperature points for T_{case}

$$T_{case} = \frac{\sum_{1}^{i} T_i}{n} \tag{3.3}$$

Maximum permitted available operating temperatures for electronic devices are calculated in below.

ED 1:

$$T_{junction} = T_{case\max} + \theta_{jc} q \tag{3.4}$$

$$130°C = T_{case\max} + (64°C/W)(0.65W) \tag{3.5}$$

$$T_{casemax} = 88.4°C \quad (3.6)$$

ED 2:

$$T_{junction} = T_{casemax} + \theta_{jc} q \quad (3.7)$$

$$150°C = T_{casemax} + (15°C/W)(1.4W) \quad (3.8)$$

$$T_{casemax} = 129°C \quad (3.9)$$

ED 3:

$$T_{junction} = T_{casemax} + \theta_{jc} q \quad (3.10)$$

$$225°C = T_{casemax} + (2.5°C/W)(58W) \quad (3.11)$$

$$T_{casemax} = 80°C \quad (3.12)$$

ED 4:

$$T_{junction} = T_{casemax} + \theta_{jc} q \quad (3.13)$$

$$175°C = T_{casemax} + (7.5°C/W)(12W) \quad (3.14)$$

$$T_{casemax} = 85°C \quad (3.15)$$

ED 5:

$$T_{junction} = T_{casemax} + \theta_{jc} q \quad (3.16)$$

$$165°C = T_{casemax} + (56°C/W) + (1W) \quad (3.17)$$

$$T_{casemax} = 109°C \quad (3.18)$$

ED 6:

$$T_{junction} = T_{casemax} + \theta_{jc} q \quad (3.19)$$

$$175°C = T_{casemax} + (0.4°C/W)(0.1W) \quad (3.20)$$

$$T_{case\max} = 174.96°C \quad (3.21)$$

Table 3.2 indicates that reliable operating temperatures of the cases for the six electronic devices.

Table 3.2. $T_{case\max}$ of electronic devices

Component	$T_{case\max}$ ºC	Heat Flux W/cm^2
ED 1	88.4	5.43
ED 2	129	1.21
ED 3	80	619.6
ED 4	85	1.86
ED 5	109	0.15
ED 6	174.96	0.1

The lowest $T_{case\max}$ is the critic temperature for this study because this is the first to be exceeded. ED 3 has the lowest $T_{case\max}$ and the biggest heat flux compared with other electronic devices. Therefore, ED 3 must be the critical component. In the numerical analyses, ED 3 is proposed to cool and tried to stay in below at the critical conditions.

3.3. Channel Geometries and Specifications

3.3.1. Straight Channel Geometry

Wavy channels are compared to the straight channel numerically and the optimum geometry in terms of pressure drop/pump power and heat transfer performance is found. This geometry can be seen in Figure 3.7.

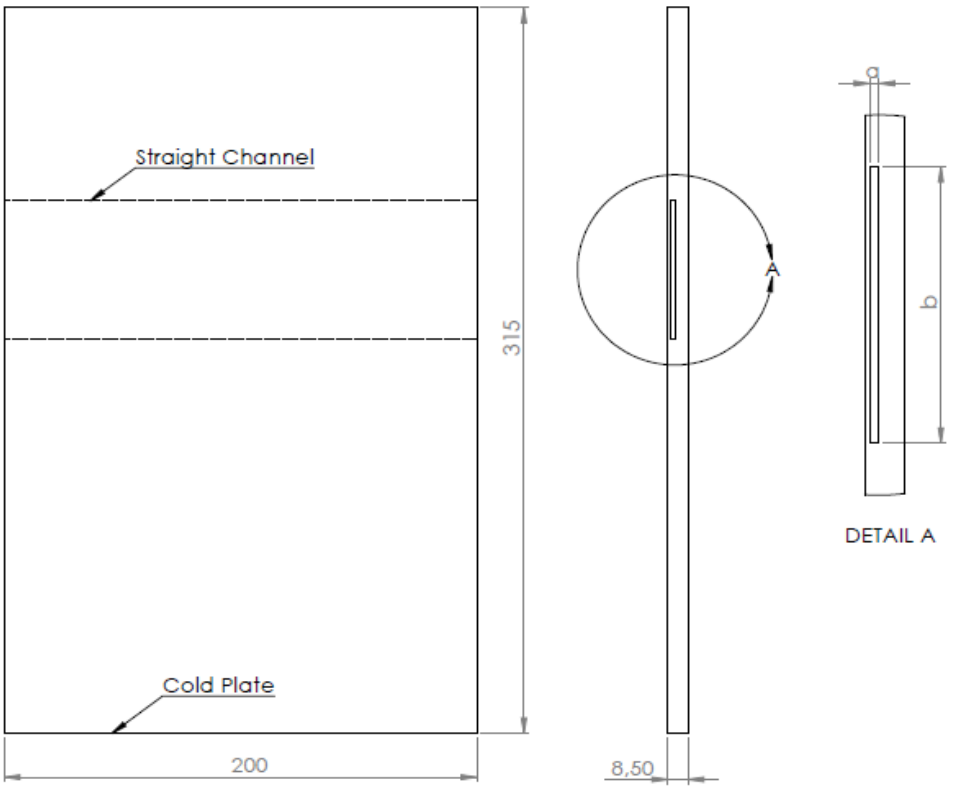

Figure 3.7. The straight channel geometry

The cross sectional area of the wavy channels is same as the straight channel. The length of the channel in the cold plate is 200 mm. Additionally, in order to obtain fully developed laminar flow conditions at the entrance of the cold plate, channel is virtually extended upstream of the cold plate and only flow is solved through this part. Equation 3.22 shows hydrodynamic entry length;

$$L \approx 0.06\,\mathrm{Re}\,D_h \qquad 3.22$$

where L is hydrodynamic entry length (m), D_h is hydraulic diameter (m) and Re is the Reynolds number.

$$\mathrm{Re} = \frac{\rho V_{mean} D_h}{\mu} \qquad 3.23$$

where ρ is density (kg/m^3), V_{mean} is average velocity (m/s), D_h is hydraulic diameter (m) and μ is dynamic viscosity (kg/m.s).

$$D_h = \frac{4A_c}{P} \tag{3.24}$$

where A_c is the cross-sectional area (m^2) and P is the wetted perimeter (m).

3.3.2. Wavy Channel Geometry

Wavy channel geometry is constituted by using sinusoidal passages. The profile of sinusoidal passage is given by Equation 3.25,

$$y = A\sin\left(\frac{2\pi x}{\lambda}\right) \tag{3.25}$$

where A is wave amplitude, wavelength is λ. In Figure 3.8 can be seen a sinusoidal wavy channel.

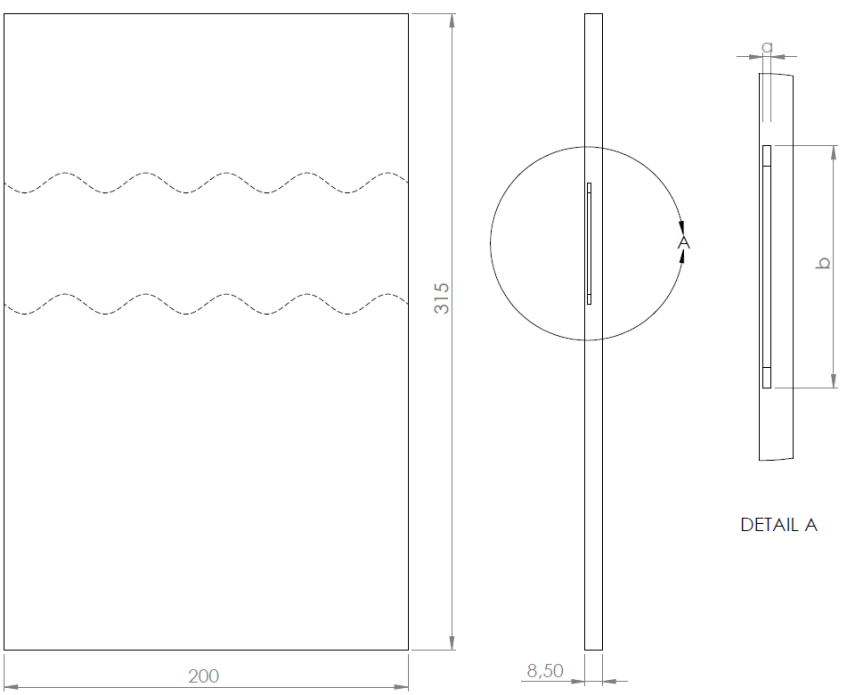

Figure 3.8. Geometry of wavy channel in cold plate

All wavy channel geometries have constant cross sectional area because phase shifting angle φ is zero. The different phase shifting angles for the wavy geometries are shown in Figure 3.9 (Rush et al. 1999).

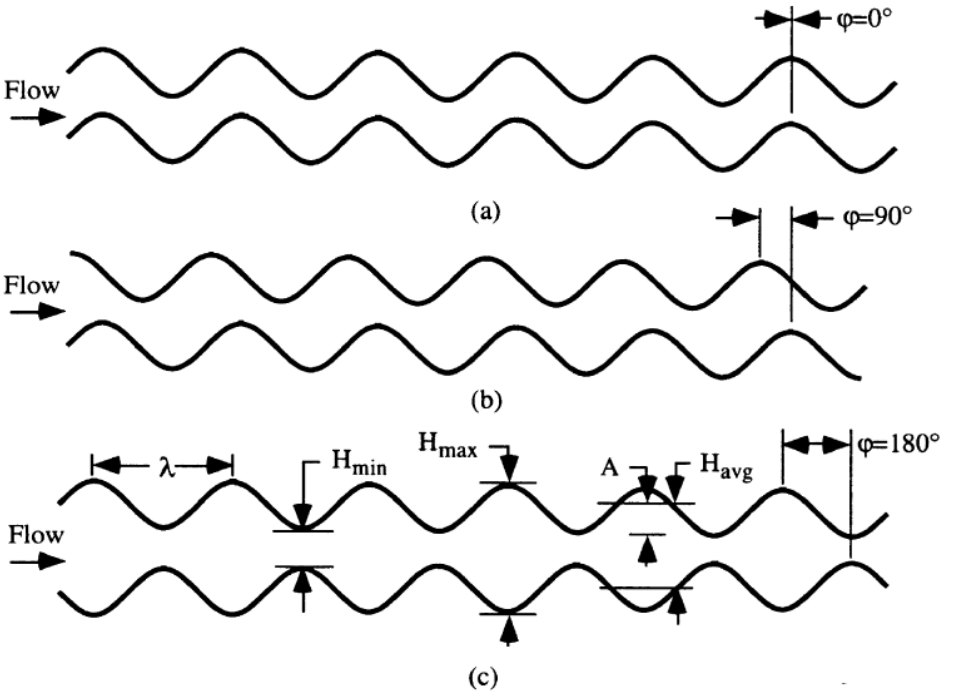

Figure 3.9. Wavy passage configurations for different phase shifting angle (a) φ=0°, (b) φ=90°, (c) φ=180° (Source: Rush et al. 1999)

In the study, some configurations are performed for different wave amplitudes, wave lengths and volumetric flow rates. Studied geometries of wavy channels are shown in Figure 3.10 in which A is wave amplitude and WL is wavelength.

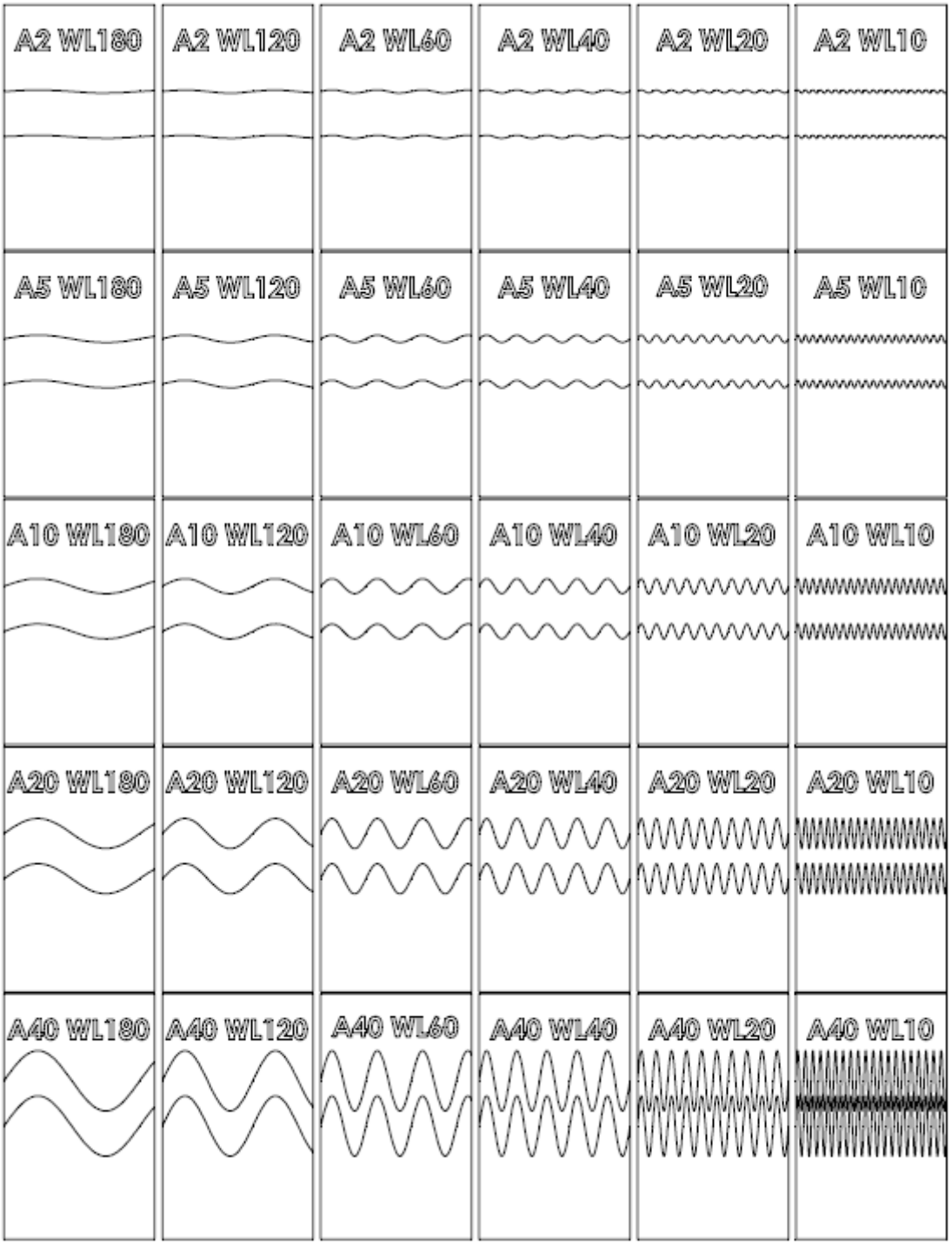

Figure 3.10. General view of wavy channel geometries

3.4. Material Properties

3.4.1. Thermo-physical Properties of Aluminum

The materials of the electronic module and the cold plate are chosen 6061-T6 alloy of aluminum in the analyses. This material has some advantages compared with the others. The Al 6061-T6 has good thermo-physical properties such as high thermal conductivity, good brazebility, good machinability properties and relatively light weight. Table 3.3 shows which thermo-physical properties of aluminum are used in the analyses.

Table 3.3. Thermo-physical properties of 6061-T6 Aluminum

Density	2700 kg/m^3
Specific Heat	871 j/kgK
Thermal Conductivity	167 W/mK

3.4.2. Thermo-physical Properties of Working Fluid

In this study, 50%-50% ethylene-glycol water mixture by volume at 20ºC is chosen for the working fluid where ethylene glycol is used as antifreeze. This mixture is widely used in the industrial applications such as heating, ventilating, air conditioning (HVAC) systems, reactor heating and cooling, electronic cooling, heat pumps and many other heat exchange systems. This fluid takes place in most heat transfer applications due to its effective heat transfer efficiency. It has a relatively lower viscosity and freezing point and relatively high boiling point. Operating range of this liquid changes between -37ºC and 111ºC. Dowcal 10 is an ethylene glycol based fluid which manufactured by Dow Inc. whose physical properties with mixing water are given in Figure 3.11.

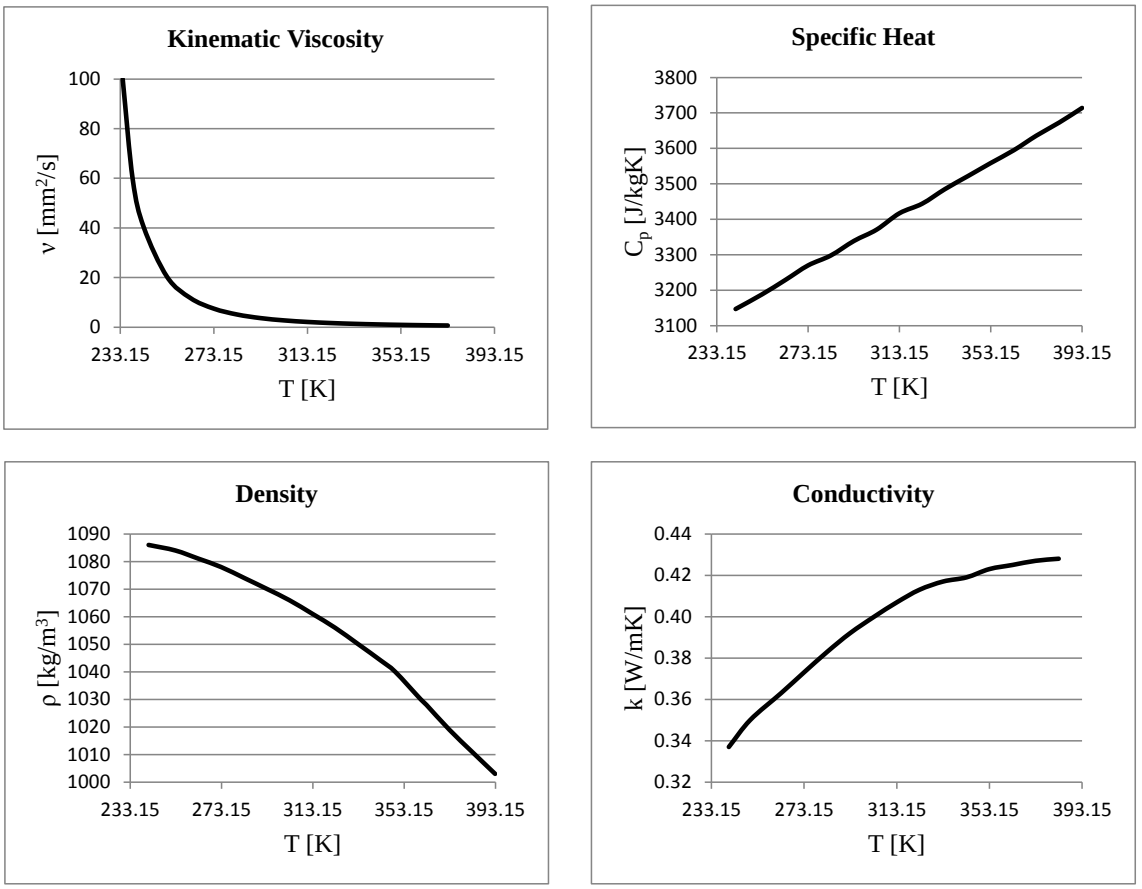

Figure 3.11. Thermo-physical properties of 50% ethylene-glycol water mixing

3.5. Boundary Conditions

3.5.1. Inlet Boundary Condition

At the inlet boundary, uniform velocity profile is employed as shown in Figure 3.12. Flows develop in the virtual channel whose entire purpose is to attain fully developed flow conditions at the entrance of the cold plate. This technique is used in all the cases. The average velocities are found from volumetric flow rates used in the calculations. The average velocities are defined at the entry of flow and only flow calculations are solved through the entrance region in order to provide fully developed laminar flow at the inlet of cold plate. Note that the temperature and the viscosity of the working fluid is constant so the properties of the working fluid are used at 20ºC. Same method is applied for both the straight and wavy to get fully developed laminar flow conditions at the cold plate. Figure 3.12 shows this boundary conditions. Only flow

calculations are performed from point A to point B, heat transfer and flow calculations are solved from point B to C.

$$u = \text{uniform velocity is defined} \tag{3.26}$$

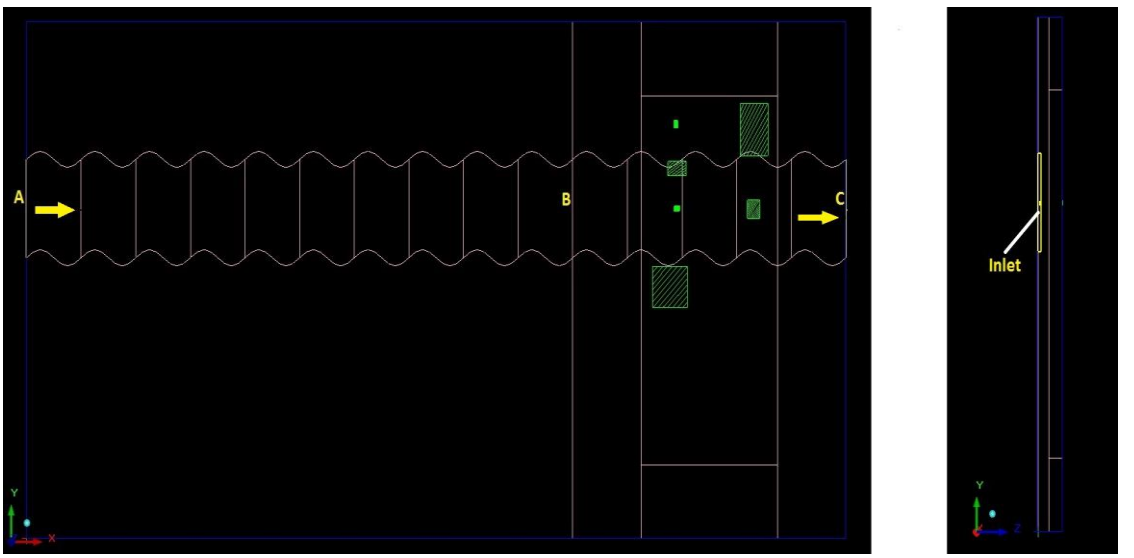

Figure 3.12. Inlet boundary condition surface in the model

3.5.2. Outlet Boundary Condition

At the outlet boundary, constant and uniform static pressure (zero gauge pressure) is employed. The outlet boundary condition surface is shown in Figure 3.13 as (2). In contrast of outlet pressure, inlet pressure will be calculated at each iteration.

$$P_{outlet} = 0(bar) \tag{3.27}$$

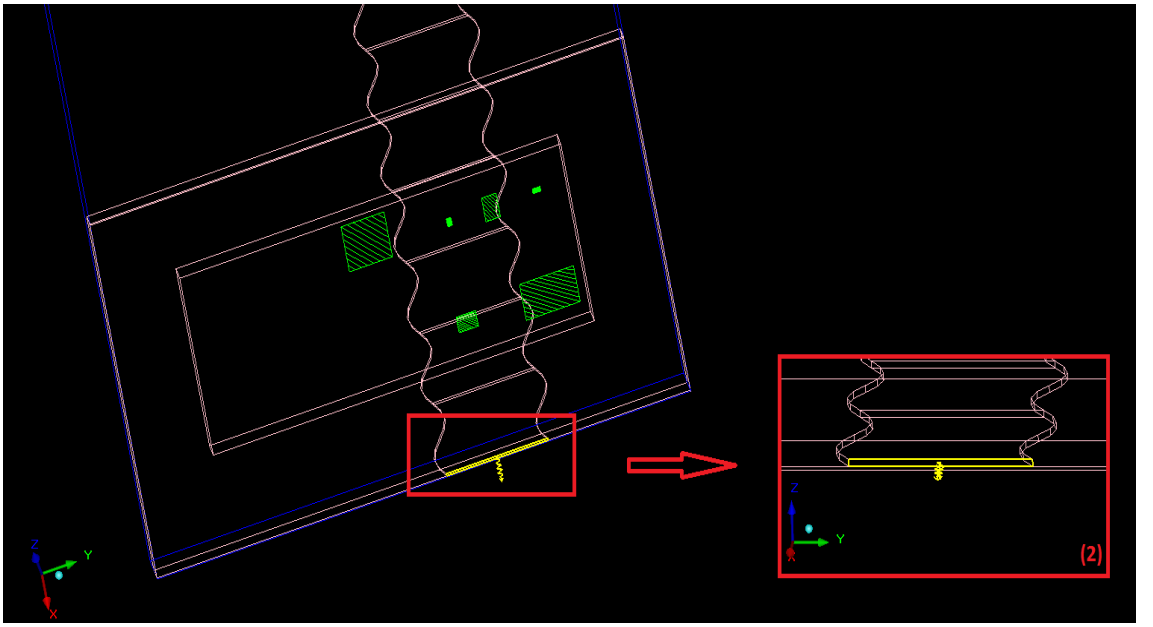

Figure 3.13. Outlet boundary condition surface in the model

3.5.3. Wall Boundary Condition

Wall boundary conditions are the limits of the solid and fluid regions. In this study, all walls of the cold plate and electronic module have either thermal or hydraulic boundary conditions. All walls except one of them are assumed to be adiabatic walls. Adiabatic walls provide perfect insulation against to heat flow. Figure 3.14 shows insulated walls as red surfaces. Constant heat flux is dissipated from the interface between electronic components and aluminum module surface. Blue surfaces has only no-slip hydraulic boundary condition.

$$\frac{\partial T}{\partial n} = 0 \qquad 3.28$$

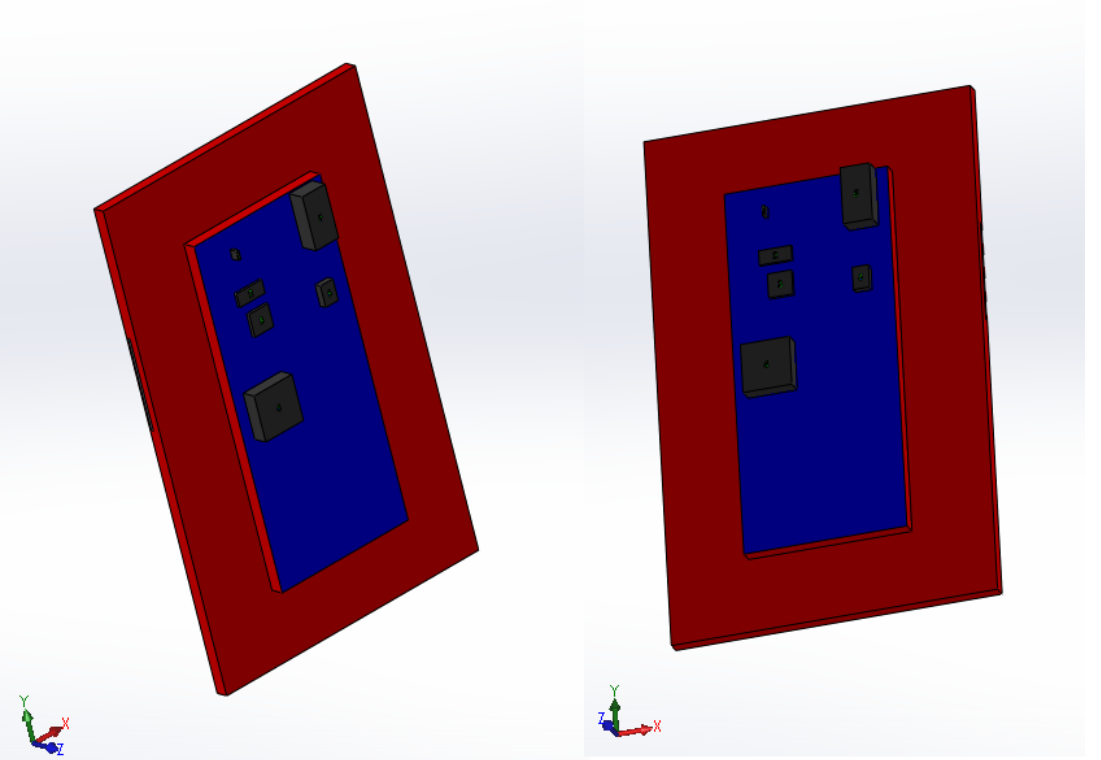

Figure 3.14. Wall boundary conditions in the model

3.6. Governing Equations

In the numerical study, equations of energy, momentum and continuity (from there pressure field) are solved. These are called governing equations. The model is performed with the following assumptions,

- The flow is steady and laminar
- No thermophysical variation with temperature ,constant density
- The working fluid is incompressible, viscous and Newtonian.

- Continuity Equation

The equation for conservation of mass, or continuity equation, can be written as follows,

$$\frac{\partial \rho}{\partial t} + \nabla\left(\rho \vec{V}\right) = 0 \qquad 3.29$$

For an incompressible fluid, steady flow and constant ρ (density), the equation 3.30 becomes

$$\nabla \vec{V} = 0 \tag{3.30}$$

- Momentum Equations

The momentum equations govern the dynamic behavior of fluid in motion and can be described by

$$\frac{\partial}{\partial t}\left(\rho \vec{V}\right) + \nabla\left(\rho \vec{V}\vec{V}\right) = -\nabla P + \nabla\left(\bar{\bar{\tau}}\right) + \rho \vec{g} + \vec{F} \tag{3.31}$$

where P is the static pressure, $\bar{\tau}$ is the stress tensor, and $\rho \vec{g}$ is the gravitational body force, $\vec{F}$ contains other source terms such as resistances, sources, etc. For our assumptions, the momentum equation is simply

$$\rho\left(\vec{V}.\nabla \vec{V}\right) = -\nabla P + \mu \nabla^2 \vec{V} \tag{3.32}$$

- Energy Equation

The energy equation for a fluid region can be written in terms of sensible enthalpy h as

$$\frac{\partial}{\partial t}(\rho h) + \nabla\left(\rho h \vec{v}\right) = \nabla\left[\left(k + k_t\right)\nabla T\right] + S_h \tag{3.33}$$

where k is the molecular conductivity, k_t is the conductivity due to turbulent transport but it is ignored in the study because of laminar flow, the source term S_h includes any defined heat sources. For our assumptions, the energy equation is simply

$$\vec{V}.\nabla T = \frac{k}{\rho c_p} \nabla^2 T \tag{3.34}$$

In conducting solid regions, solver solves a simple conduction equation that includes the heat flux due to conduction and volumetric heat sources within the solid;

$$\frac{\partial}{\partial t}(\rho h) = \nabla(k \nabla T) + S_h \qquad 3.35$$

where the ρ is density, k is conductivity, T is temperature and S_h is the volumetric heat source.

3.7. Overview of Numerical Solution

The governing equations of fluid flow and heat transfer where used to solve model are shown in Equations 3.30, 3.31, and 3.33. These equations are nonlinear partial differential equations which cannot be solved by using analytical methods. Hence, the equations should be solved numerically.

Firstly, the solution of the problem begins with dividing the computational domain into small volumes which are called meshes. The meshing operation for this study is performed by using commercial software as Ansys-Icepak. The unstructured hexagonal meshes are generated for this problem. The details of mesh operating are mentioned in Section 3.8.

In the study, Ansys Icepak will solve the governing equations for mass, momentum, energy and other scalars. A control volume based technique is used to solve problem, which consists of ;

- Division of the domain into discrete control volumes using a computational grid.
- Integration of the governing equations on the individual control volumes to construct algebraic equations for the discrete dependent variables (unknowns) such as velocities, pressure, temperature, and conserved scalars.
- Linearization of the discretized equations and solutions of the resultant linear equation system to yield updated values of the dependent variables.

The governing equations are solved iteratively because these equations are non-linear and coupled. Iterations must continue until the differences between consecutive solutions are small enough. This is called a “converged solution”. Each iteration is performed with the following steps,

- Fluid properties are updated, based on the current solution.

- Solve the momentum equations, using current values for pressure and face mass fluxes (in order to update the velocity field).
- Solve the pressure correction equation using the recently obtained velocity field and the mass-flux. This pressure correction equation is then solved to obtain the necessary corrections to the pressure and velocity fields and the mass fluxes such that continuity is satisfied.
- Equation of energy is solved using the previously updated values of the other variables.
- Check for convergence of the equations.

These steps are continued until the convergence criteria are met. The flow chart of the solution method is denoted in Figure 3.15.

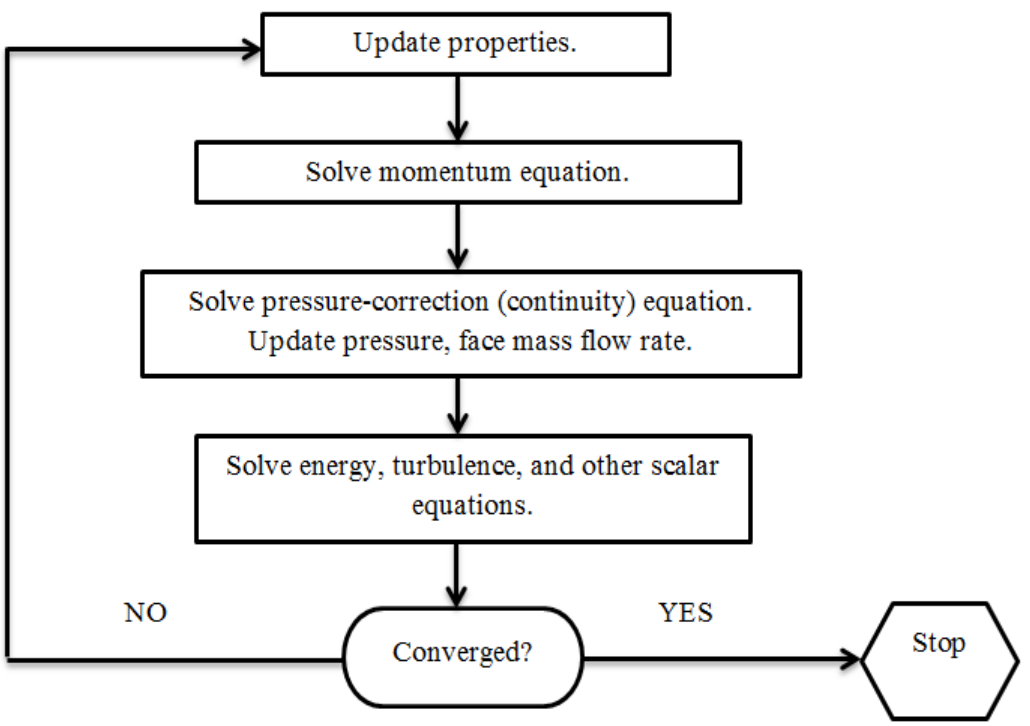

Figure 3.15. Overview of the solution method
(Source: Ansys 14.5 Icepak User's Guide)

3.8. Mesh Generation and Computational Details

3.8.1. Mesh Generation

Firstly, to solve the studied problem, the geometry must be divided into small domains which are called as grids or meshes. The mesh generation for this cooling problem is done by using Ansys Icepak mesh generation module.

Hexahedral meshing procedure with using hexa unstructured mesher is applied for the problem. The max x size, max y size and max z size values are set in the model. The grids in the channel are generated tighter than others because of flow calculations. Uniform mesh is used to create the mesh generation for the numerical domain. Mesh generation in x, y and z direction for the straight channel model by applying uniform mesh is shown in Figure 3.16. Mesh generation module constructs control volumes around the nodes from element sector so the number of control volumes is equal to the number of nodes. The number of nodes is 4.9 million for the straight channel model.

The pressure difference (pressure drop) is calculated by subtracting the average pressure at the inlet face (P_{inlet}) from average pressure at outlet face (P_{outlet}) of cold plate. The pressure drop equation is given as;

$$\Delta P = P_{inlet} - P_{outlet} \tag{3.36}$$

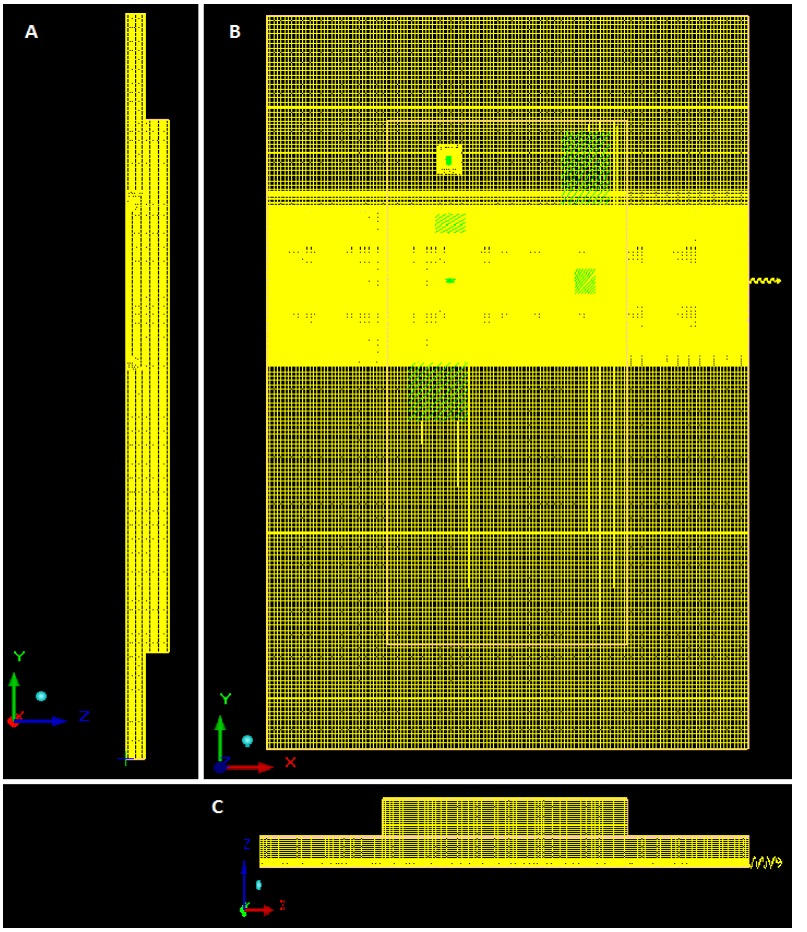

Figure 3.16. Mesh generation in the model (A-X sight, B-Z sight and C-Ysight)

A mesh independency study is performed to obtain the optimal mesh. This calculation is very important in terms of computation time and more accurate solution. The different number of mesh has been generated and optimal mesh for model is found. In Figure 3.17 shows mesh independency results.

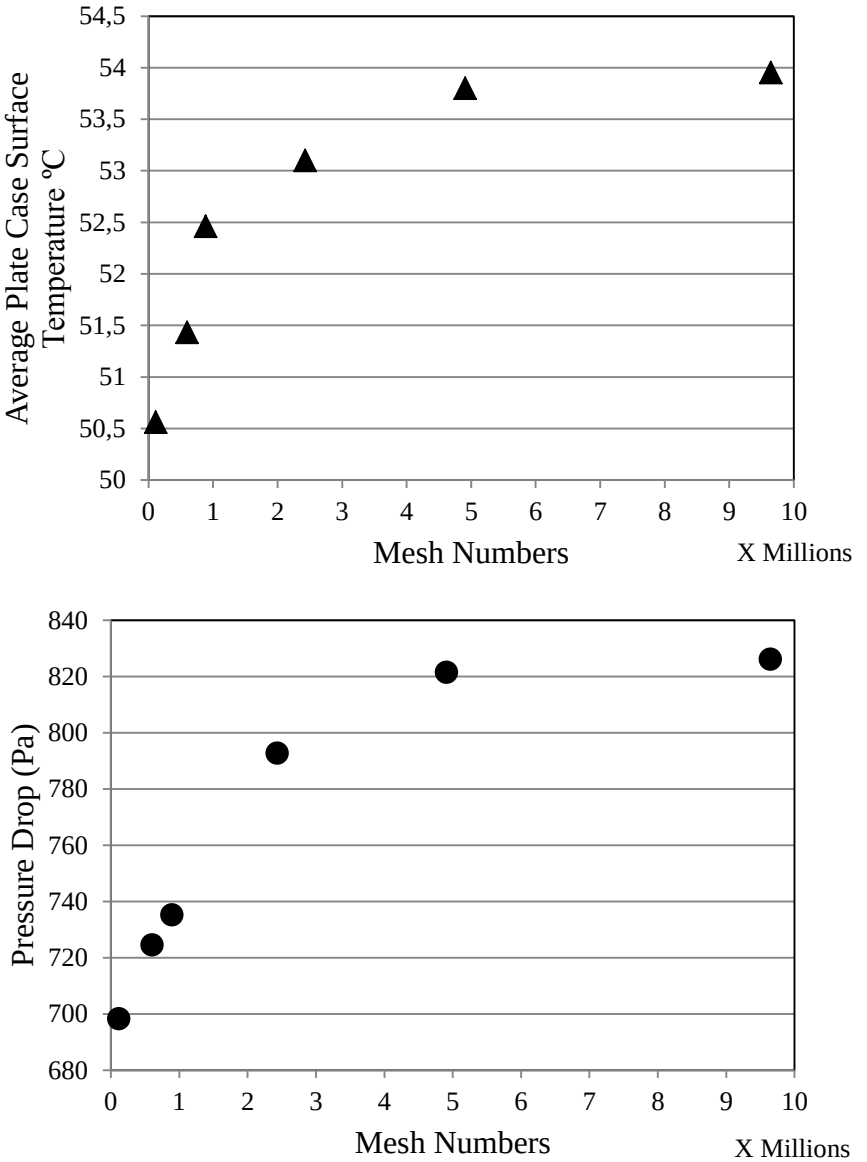

Figure 3.17. Mesh independence analyses for the straight channel geometry at Re=368

Various grids of sizes from 114000 nodes to 9.7 million nodes were employed for checking the mesh independency of the solution. The difference in the pressure drop and the average plate case surface temperature between the solutions on the meshes with 4.9 million and 9.7 million nodes was found to be about 0.55% and 0.3%. Therefore, 4.9 million nodes were used to solve the problem in order to save computing time and memory.

Mesh independency analyses were performed for other wavy channel geometries. In Figure 3.18 shows this analyzes for the sinusoidal wavy channel whose amplitude is 40 mm and wavelength is 120 mm.

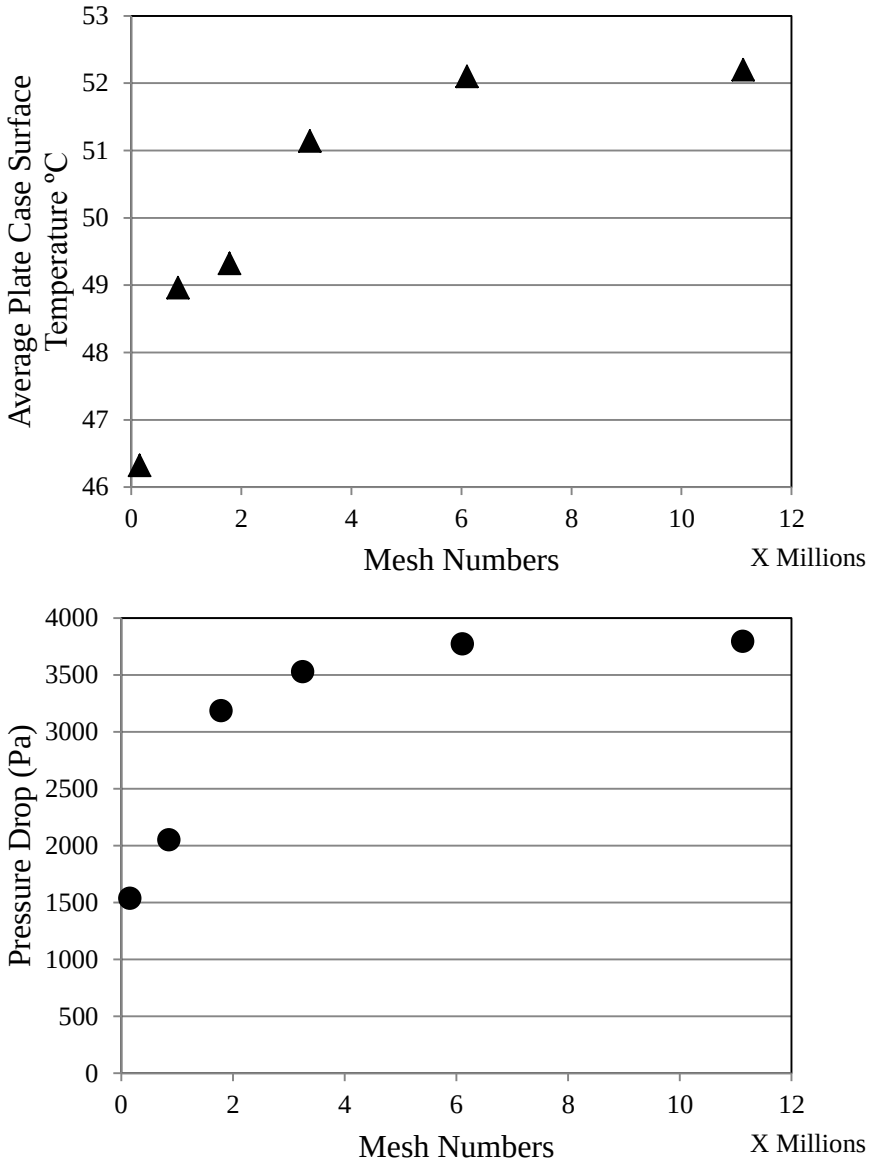

Figure 3.18. Mesh independence analyses for sinusoidal wavy channel geometry A =40 mm λ=120 mm at Re=368

Various grids of sizes from 152000 nodes to 11.2 million nodes were employed again for checking the mesh independency of the solution. The difference in the pressure drop and the average plate case surface temperature between the solutions on the meshes with 6.1 million and 11.2 million nodes was found to be about 0.6% and 0.2%. Therefore, 6.1 million nodes were used to solve for the wavy channel problem in order to save computing time and memory.

3.8.2. Computational Details

In the study, a relative error ε of less than 10^{-7} was assumed as the convergence criteria for continuity, velocities and energy equations. When ε reaches value of $<10^{-7}$, the iterating procedure is stopped for all solutions. The converged numerical criteria for laminar case can be written as:

- Residual for continuity : $R_c=10^{-7}$
- Residual for velocities in x, y and z directions : $R_v:10^{-7}$
- Residual for energy : $R_e:10^{-7}$

During the iterations, it is necessary to reduce the change of a variable from one iteration to the next one. If this change is not reduced (relaxed) by a certain factor, solution usually diverges from the start. That means that an under-relaxation factor must be employed for each equation. Constant under-relaxation factors are used in the solver and they are listed as;

- Pressure : 0.3
- Momentum : 0.7
- Energy : 1

CHAPTER 4

RESULTS AND DISCUSSION

The main purpose of this thesis is to obtain optimum wave geometry numerically in terms of heat transfer performance and pump power (or pressure drop) as a part of restricted flow rates. Therefore, the reference channel model is defined as the straight channel compared to different sinusoidal wavy channels. In this chapter, values of temperature and pressure drop obtained from numerical analyses are discussed and evaluated.

4.1. Results of the Straight Channel Geometry

The straight channel geometry is performed whose features are given in Chapter 3. The temperature and pressure drop values of the model are obtained for different flow rates between 0.05 and 2.5 liter per minute (lpm). According to the definition of Reynolds number given in Equation 3.23. Re numbers are between 7 and 368. To calculate pump power of the model, Equation 4.1 is applied as below. In this equation fluid density is taken as 1, since it is kept constant in entire thesis and therefore, it is irrelevant to the problem.

$$W_{pump} = \dot{\vee} \Delta P \tag{4.1}$$

where $\dot{\vee}$ is volumetric flow rates and ΔP is the pressure drop where in the cold plate.

For a better visualization, the analyses results of the straight channel model are given as follows.

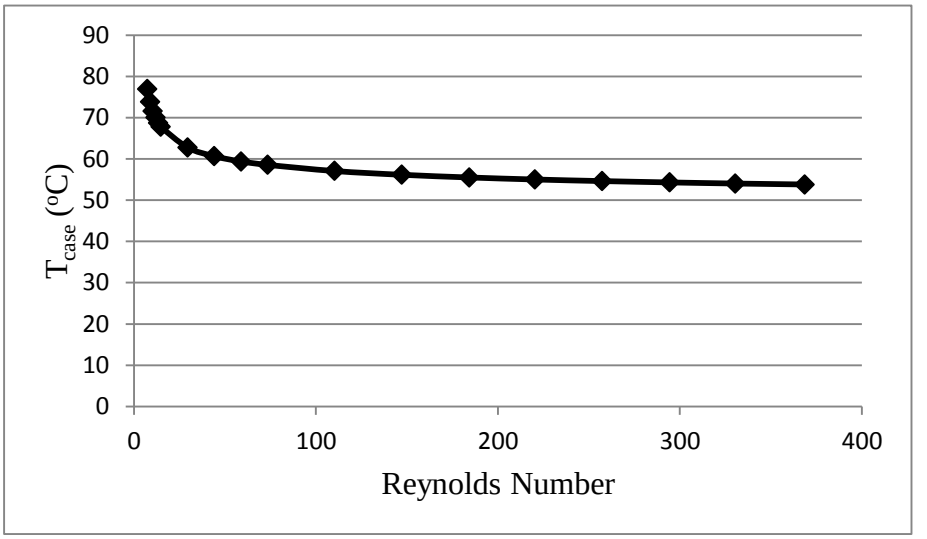

Figure 4.1. Variation in T_{case} with Re number

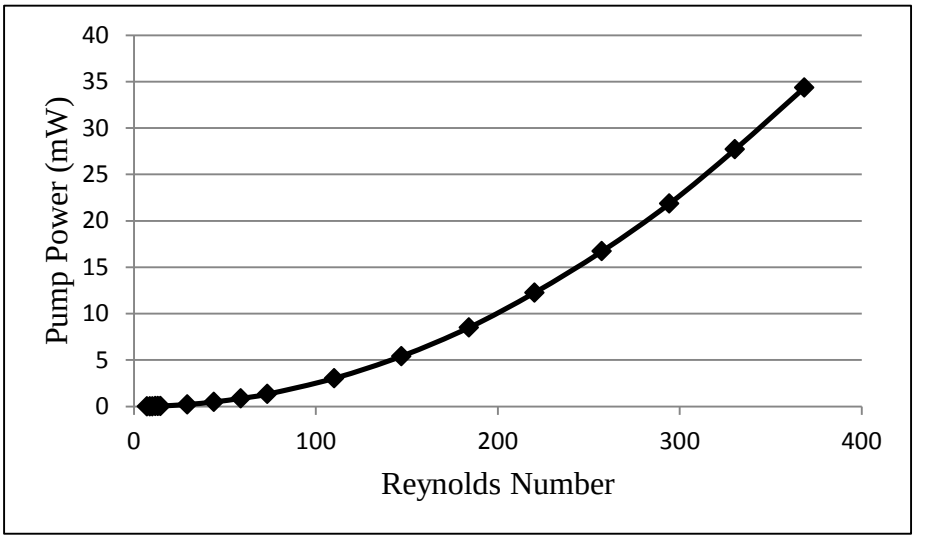

Figure 4.2. Variation in W_{pump} with Re number

In Figure 4.1 and Figure 4.2 show temperature and pressure drop values for the straight channel model. These results are used reference values for the comparing sinusoidal wavy channel geometries.

4.2. Results of the Sinusoidal Wavy Channel Geometry

The sinusoidal wavy channel geometries are investigated and their features are given in Chapter 3. Some configurations of sinusoidal wavy channel are shown in Figure 3.10 but all the geometries shown are not solved because of the fact that trends

from the earlier solved geometries indicate that their solutions are very away from the optimal solution any way. Figure 4.3 shows the sinusoidal channel geometries performed in this study.

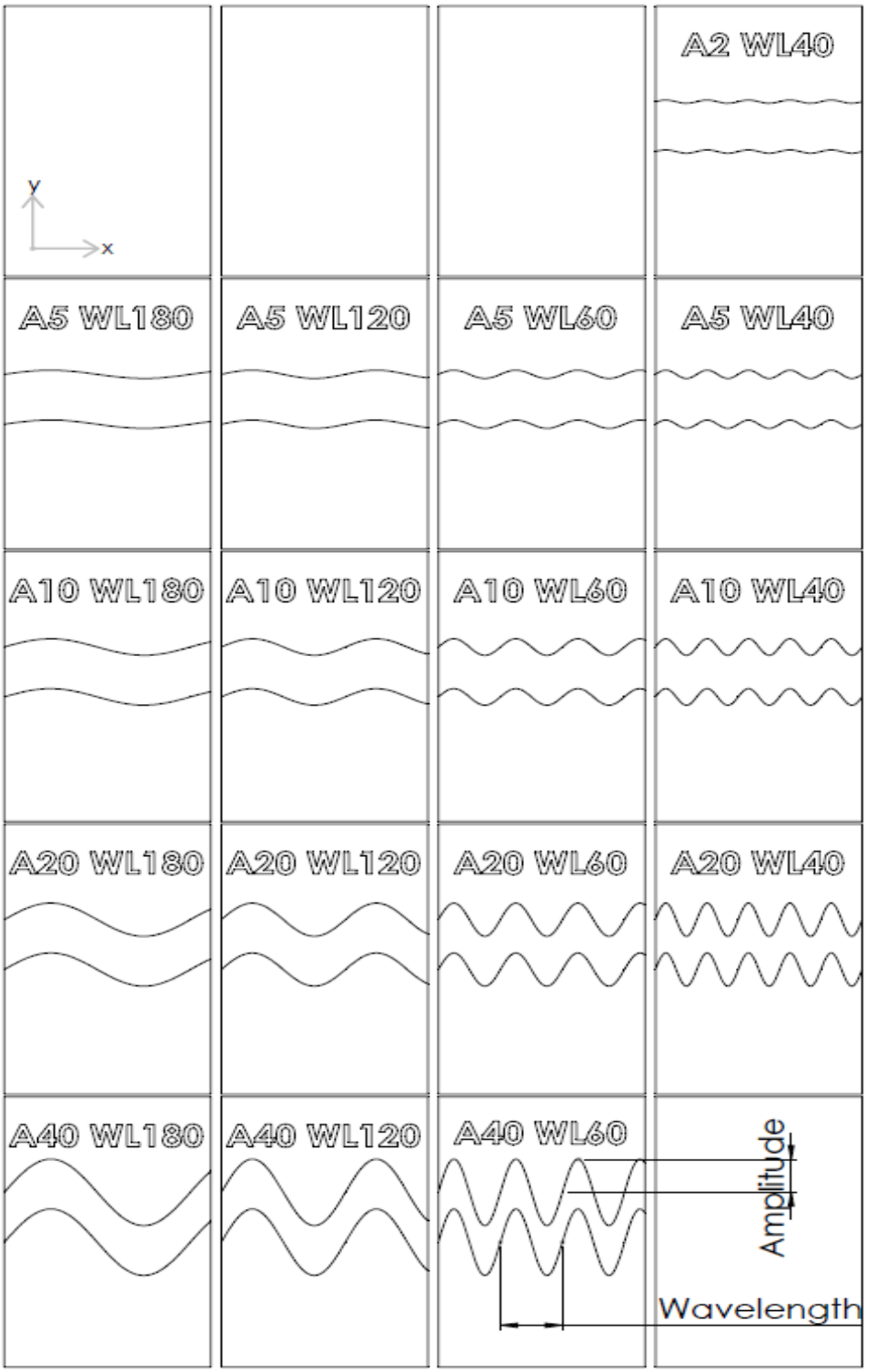

Figure 4.3. Performed the sinusoidal wavy channel geometries in the study

Some dimensionless numbers are defined to obtain information about the performance of models.

A dimensionless performance factor number (PF) is described to characterize overall performance (the enhancement in both heat transfer and pump power), which compares the all performance of sinusoidal wavy channel with the straight channel based on the conditions. The PF is calculated for all cases based on the numerical results for T_{case} and W_{pump}. Equation 4.2 is used for calculation of PF.

$$PF = \frac{\dfrac{T_{case\max} - T_{case}}{T_{case\max} - T_{ref}}}{\dfrac{W_{pump}}{W_{pumpref}}} \qquad 4.2$$

where $T_{case\max}$ is the permitted available operating temperature of ED 3 which calculated in chapter 3, T_{case} is average surface temperature of ED 3 for the sinusoidal wavy channel, T_{ref} is average surface temperature of ED 3 for the reference straight channel, W_{pump} is pump power obtained from the solution of the sinusoidal wavy channel geometry and $W_{pumpref}$ is pump power obtained from the solution of the reference straight channel geometry.

A dimensionless temperature ratio (TR) is another performance parameter defined in this thesis and is used to observe thermal performance, which compares the performance of sinusoidal wavy channel geometry with the straight channel. Equation 4.3 is used for calculation of TR.

$$TR = \frac{T_{case\max} - T_{case}}{T_{case\max} - T_{ref}} \qquad 4.3$$

A dimensionless pump power ratio (WR) is another performance parameter defined in this thesis and is used to observe pump power performance, which compares the performance of sinusoidal wavy channel geometry with the straight channel based on the conditions. Equation 4.4 is used to calculation of WR.

$$WR = \frac{W_{pump}}{W_{pumpref}} \qquad 4.4$$

4.2.1. Effect of Wave Amplitude

For the different wave amplitude, thermal performance, pump power performance and the overall performance of the model are given in the related figures.

The heat transfer performance of sinusoidal channel is same with the straight channel where the *TR* is equal to 1. Once the *TR* is bigger than 1, it indicates a heat transfer enhancement in a wavy channel compared to the straight channel. The results of the *TR* values are shown in Figure 4.4, Figure 4.5, Figure 4.6 and Figure 4.7. Each of these graph includes results from wavy channels which have the same wavelength. It is interesting to note that results of wavelength 40 mm (Figure 4.4) peaks for small Re numbers in the range Re=40 to 75.

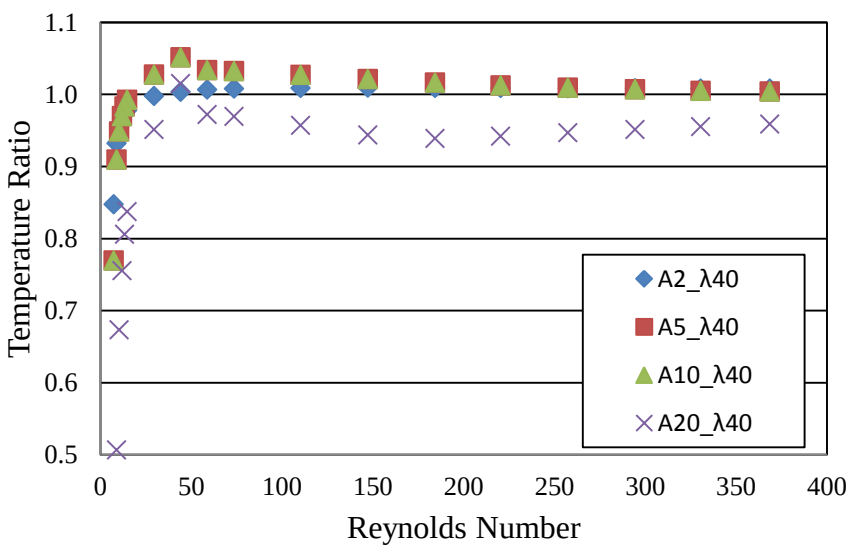

Figure 4.4. Variation in TR with Re for λ =40 mm

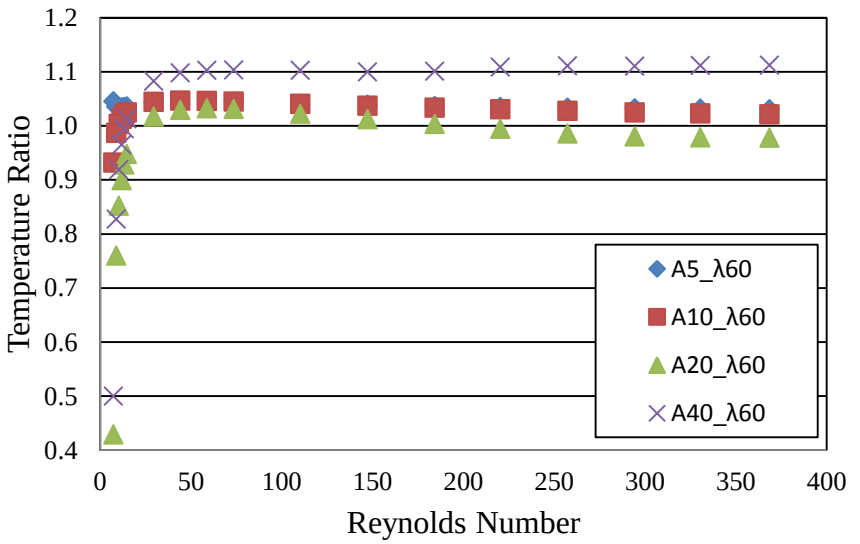

Figure 4.5. Variation in *TR* with Re for λ =60 mm

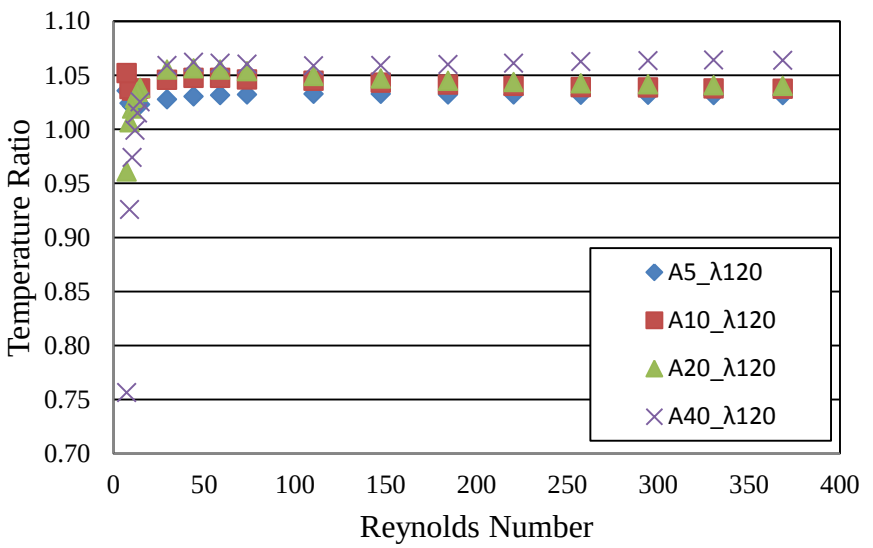

Figure 4.6. Variation in *TR* with Re for λ =120 mm

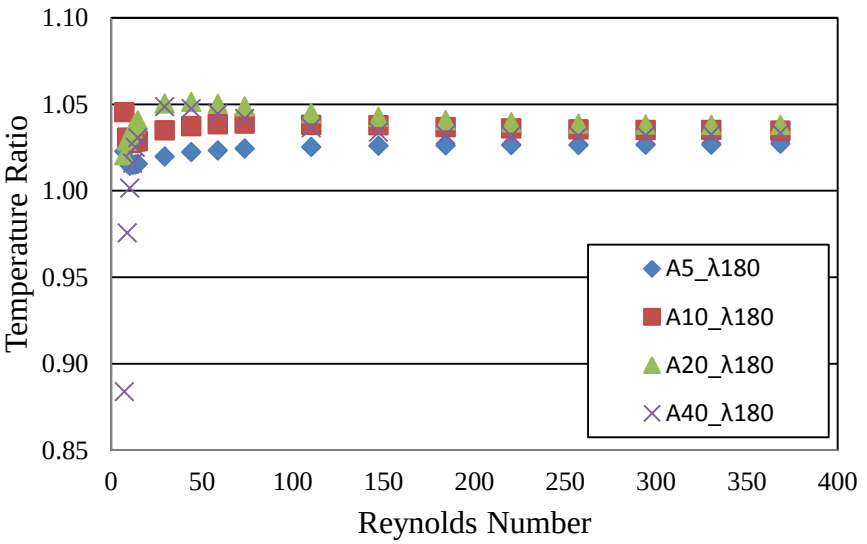

Figure 4.7. Variation in TR with Re for λ=180 mm

It can be observed from these figures, the TR usually increases with wave amplitude (A) and Re. Some sinusoidal channel profiles result in approximately 10% heat transfer enhancement such as A=40mm λ=60mm. This geometry has the biggest wave amplitude and lowest wavelength. This augmentation is very important for the critic cooling applications. Furthermore, it was investigated that the wall temperature of the channel also decreases as both A and Re increase. A affects heat transfer positively but not for all conditions. For the biggest value of A=20 with λ=40 in Figure 4.4, it influences heat transfer badly because the value of A approaches to the value of λ. This result is thought to come from the sharp corrugation in the model. In this corrugated zone, flow exhibits a stagnated flow (recirculation zone) behavior so this decreases heat transfer consequently.

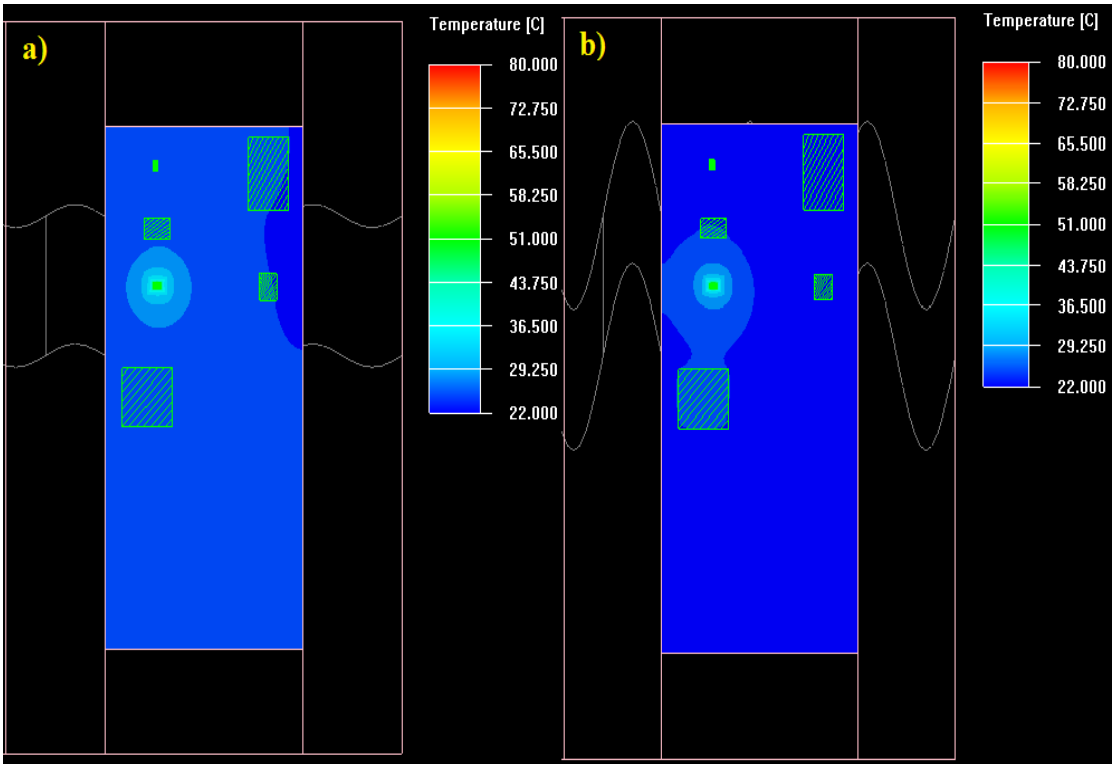

Figure 4.8. Comparison of temperature contours for different wave amplitudes a) A =5mm λ =60mm b) A =40mm λ =60mm

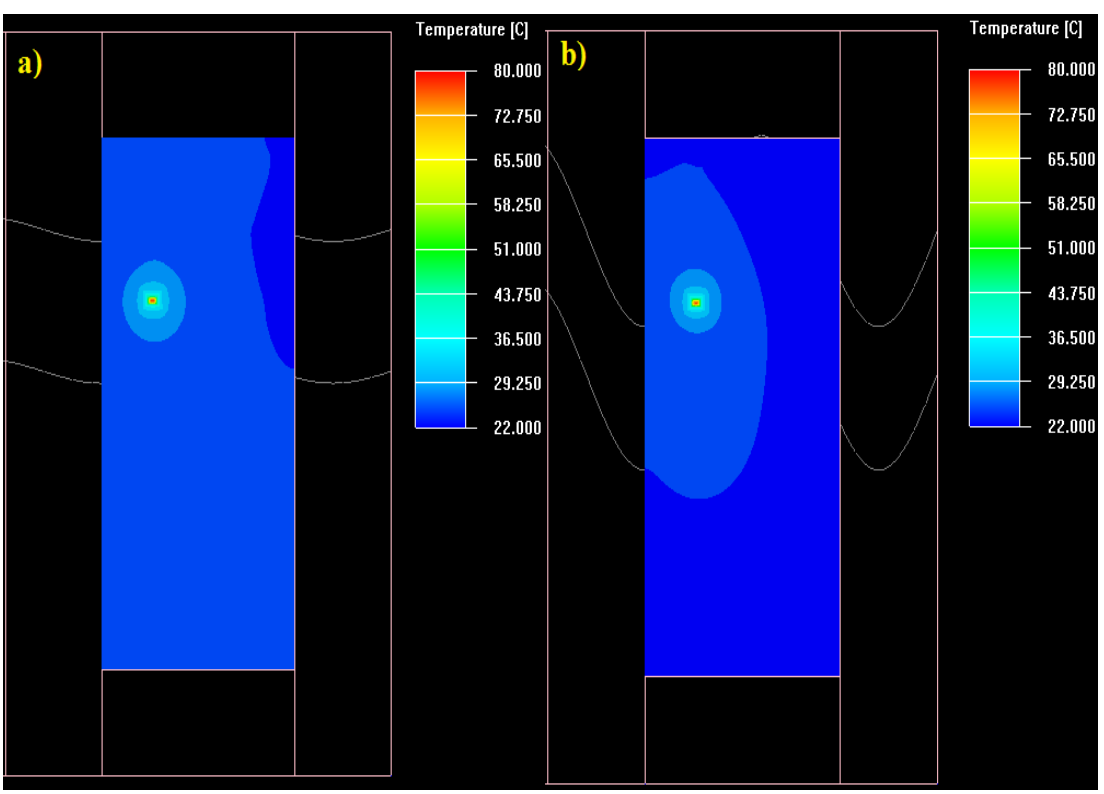

Figure 4.9. Comparison of temperature contours for different wave amplitudes a) A =5mm λ =120mm b) A =40mm λ =120mm

Figure 4.8 and Figure 4.9 show temperature contours of electronic module surface for different wave amplitudes. The surface temperature of higher amplitude geometry is lower than another. It means that the higher amplitude values supply much cooling for the system.

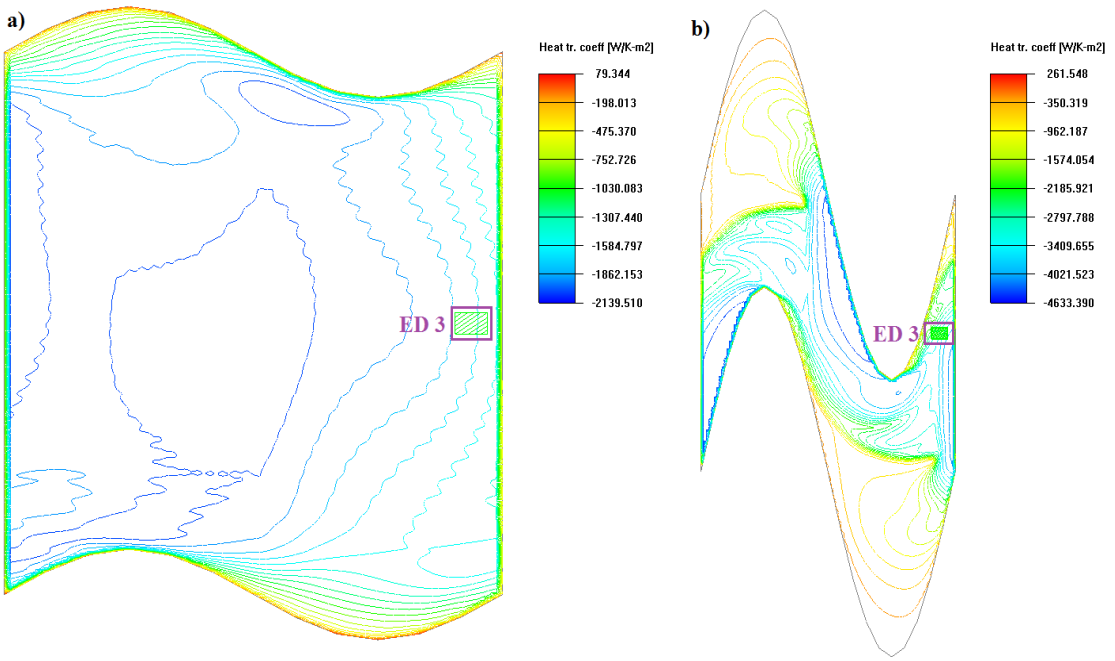

Figure 4.10. Variation of heat transfer coefficient contour line for different wave amplitudes at Re=368 a) A=5mm λ=60mm b) A=40mm λ=60mm

The heat transfer coefficient contours on the channel surface for different wave amplitudes are shown in Figure 4.10. Heat transfer coefficient of higher amplitude geometry in Figure 4.10-b is approximately two times greater than lower amplitude geometry in Figure 4.10-a. Increment of wave amplitude causes the enhancement of heat transfer. Therefore, wave amplitude effect on heat transfer can be used in practical applications especially where in the temperature limit is so important.

Grashof number is a nondimensional parameter used in the correlation of heat and mass transfer due to thermally induced natural convection at a solid surface immersed in fluid. It is defined as

$$Gr = \frac{g\beta\Delta T D^3}{\nu^2} \qquad 4.5$$

where g is acceleration due to gravity (ms^{-2}), D is hydraulic diameter (m), β is expansion coefficient of fluid (K^{-1}), ΔT is temperature difference between the surface and the bulk of fluid (K), ν is kinematic viscosity of the fluid (m^2s^{-1}).

Relative magnitudes of Gr and Re give an indication of the relative importance of natural and forced convection in the channel. Forced convection effects are usually insignificant when $Gr/Re^2>>1$ and natural convection effects can be ignored when $Gr/Re^2<<1$. When the ratio is of order of one, combined effects of natural and forced convection have to be taken into account. This is called mixed convection (Incropera et al., 2011).

In this study, the rate of Gr/Re^2 is calculated for all geometries. Gr/Re^2 changes between 0.05 and 0.0003 in the range of Reynolds number 40 and 368. It means $Gr/Re^2<<1$ so forced convection exists in this range. Gr/Re^2 changes between 0.1 and 4.5 in the range of Reynolds number 7 and 30. For these conditions, mixed convection exists in the model but natural convection effects are neglected for performed geometry at smaller Re numbers because it does not affect general deductions of numerical results. Furthermore, the flow direction is perpendicular to the gravity force in the models so the effect of gravity force is ignored.

The WR is used to evaluate performance of pump power which compares sinusoidal wavy channel geometry with the straight channel. The WR provides a way to observe energy saving possible with regard to reference model. It is expected to have a WR number smaller than 1 for all wavy channels because of the fact that their lengths are longer. Nevertheless, it is very informative to look at the relative degradations on pump powers for different wavy channels. The results of WR are shown in Figure 4.11, Figure 4.12, Figure 4.13, and Figure 4.14.

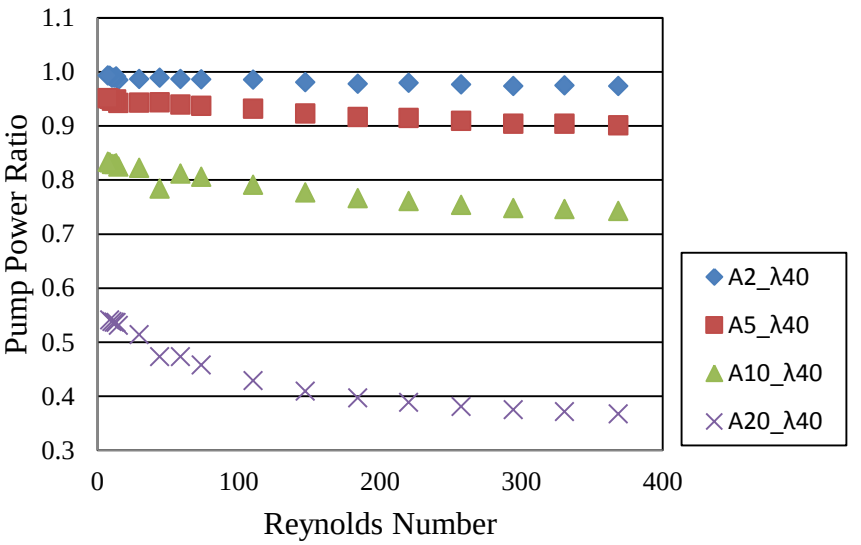

Figure 4.11. Variation in *WR* with Re for λ =40mm

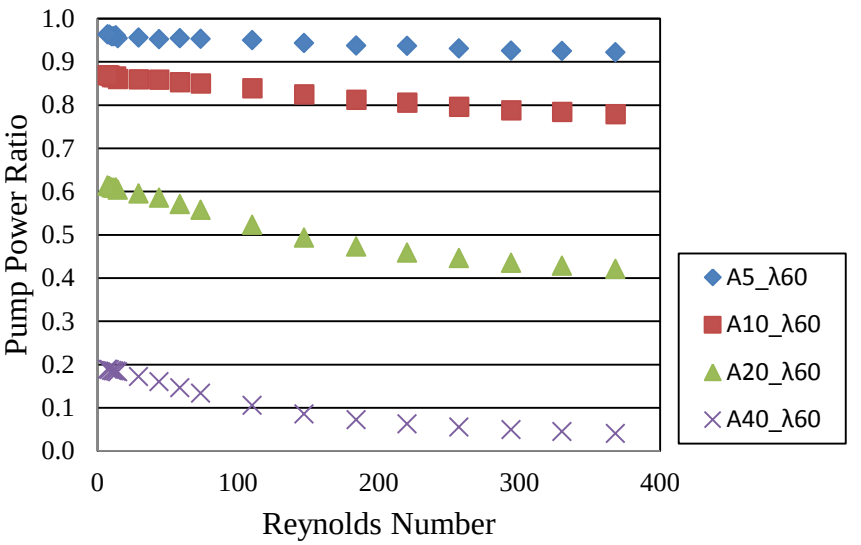

Figure 4.12. Variation in *WR* with Re for λ =60mm

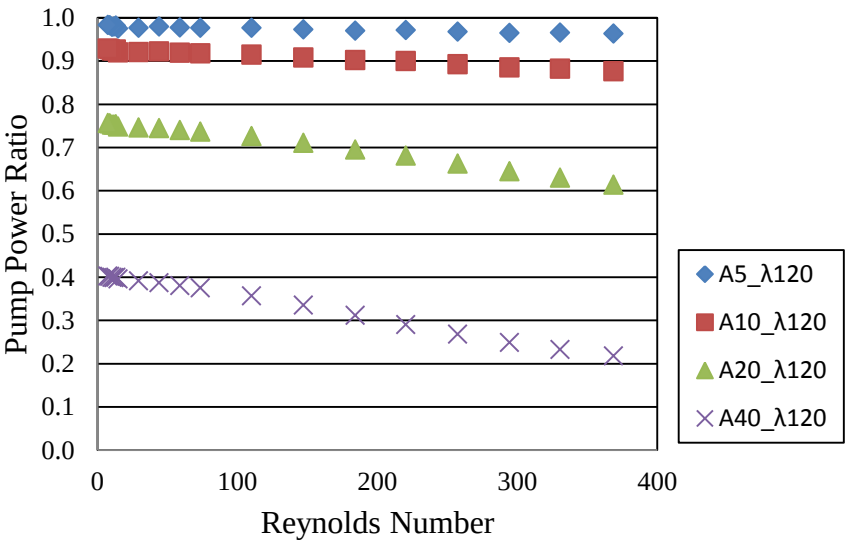

Figure 4.13. Variation in WR with Re for λ=120mm

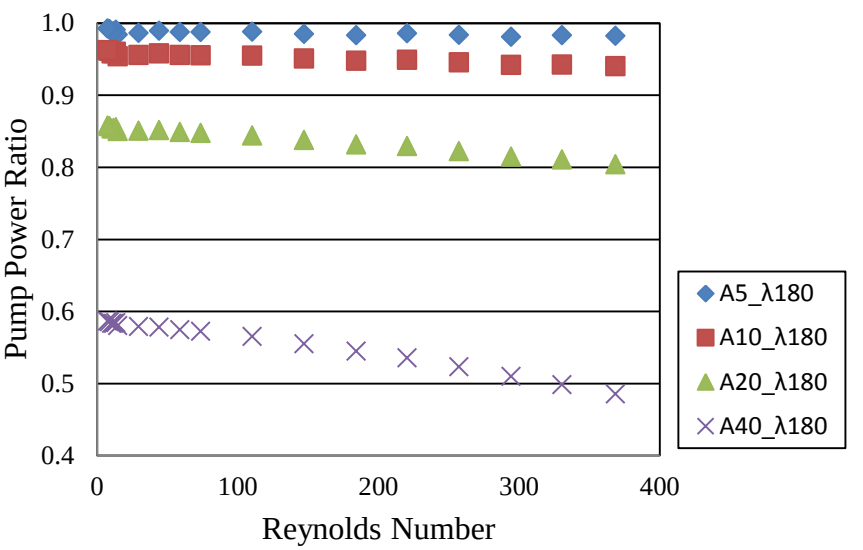

Figure 4.14. Variation in WR with Re for λ=180mm

As expected WR is always smaller than 1 which can be observed from the results. This means that the pump power of the sinusoidal wavy channel is always bigger than the straight channel. This is expected results because the pressure drop of the sinusoidal wavy channel is always bigger than the straight channel. The increasing wave amplitude (A) and Re affect the pressure drop negatively which contributes to rise of pump power compared to the straight channel.

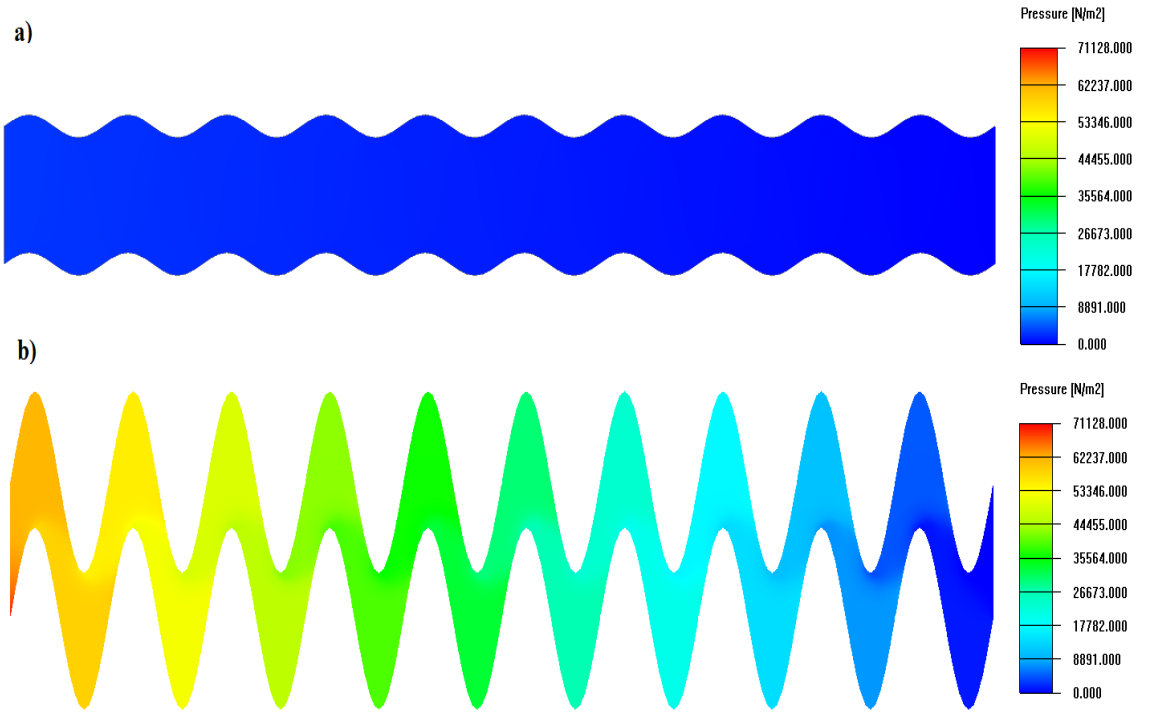

Figure 4.15. Pressure distribution for different wave amplitudes at Re=368 a) A =5mm λ =60mm and b) A =40mm λ =60mm

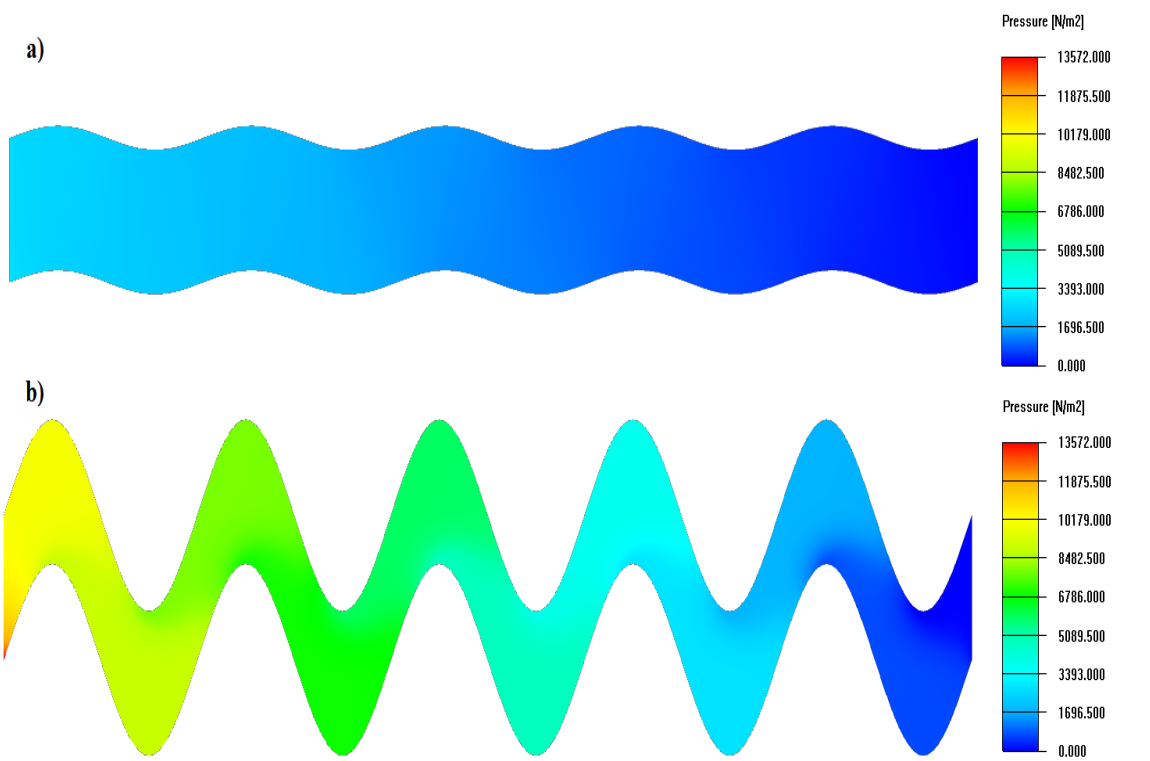

Figure 4.16. Pressure distribution for different wave amplitudes at Re=368 a) A =5mm λ =120mm and b) A =40mm λ =120mm

Pressure distribution contours for different channel geometries are shown in Figure 4.15 and Figure 4.16. Pressure drop in the channel increases with increment of wave amplitude. For the geometries in Figure 4.15, the pressure drop value of higher amplitude geometry is approximately twenty five times greater than lower amplitude geometry. This increment affects pumping power negatively because energy consumption increases with this effect.

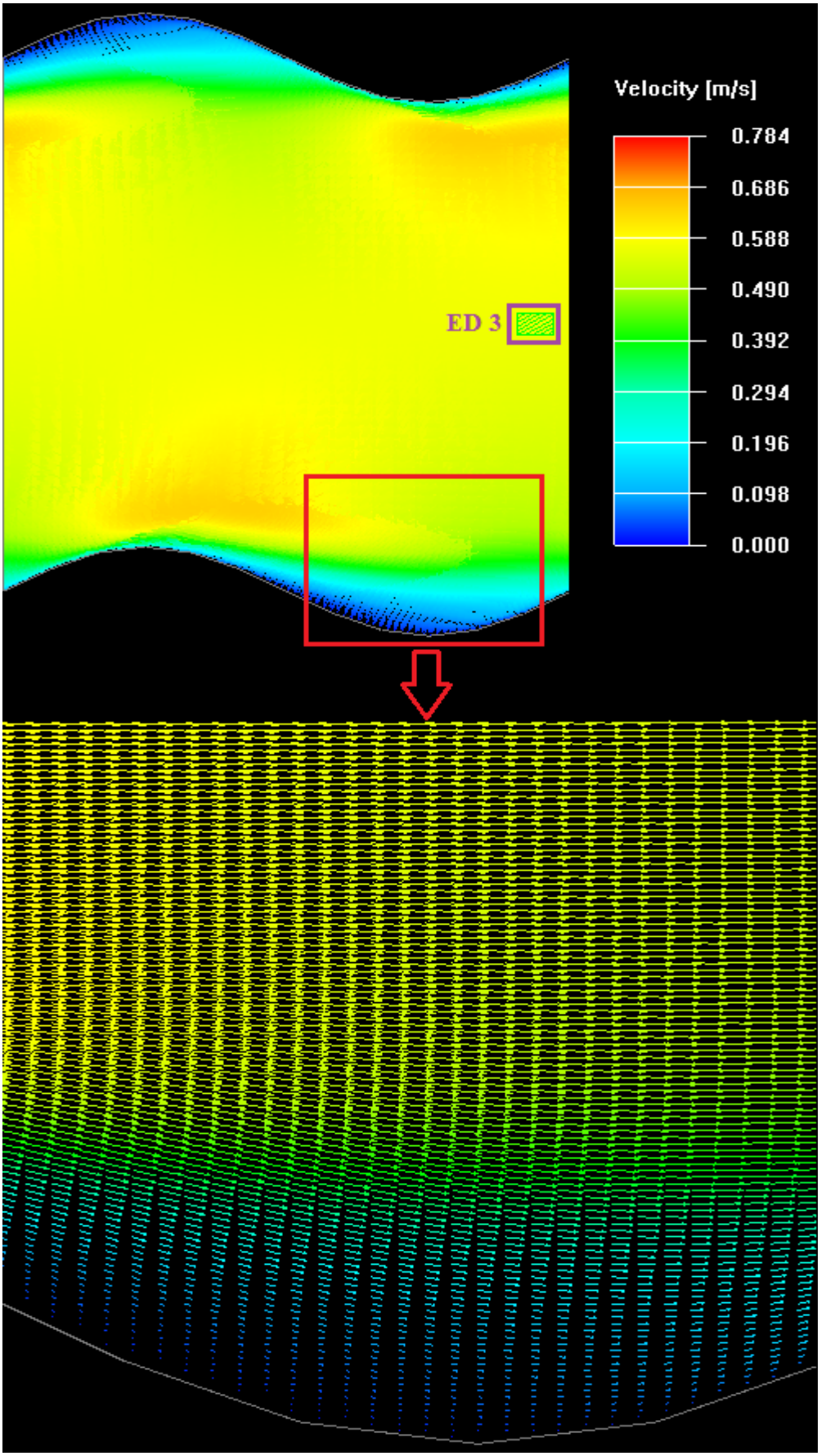

Figure 4.17. Velocity vector for A=5mm λ=60mm at Re=368

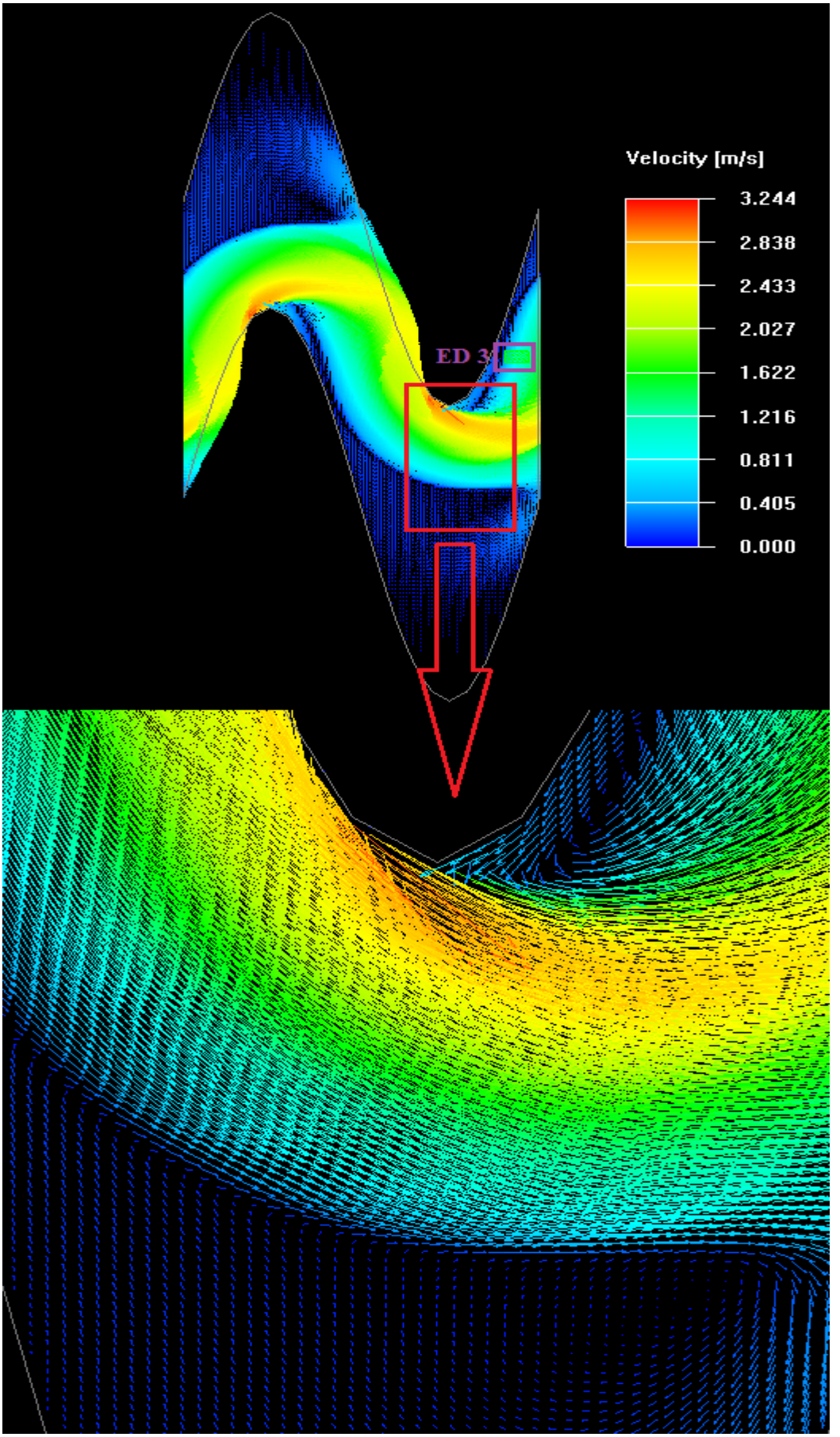

Figure 4.18. Velocity vector for A=40mm λ=60mm at Re=368

Figure 4.17 and Figure 4.18 indicate velocity vector for different wave amplitudes. Figures show that flow begins to separate from the wall at higher wave amplitudes and causes an increase in pressure drop. This can be seen in Figure 4.18.

Following charts at Figure 4.19, 4.20, 4.21, and 4.22 show the changes in factor PF . When this factor is bigger than 1, it indicates that the overall performance of the sinusoidal wavy channel geometry is better than the straight channel geometry.

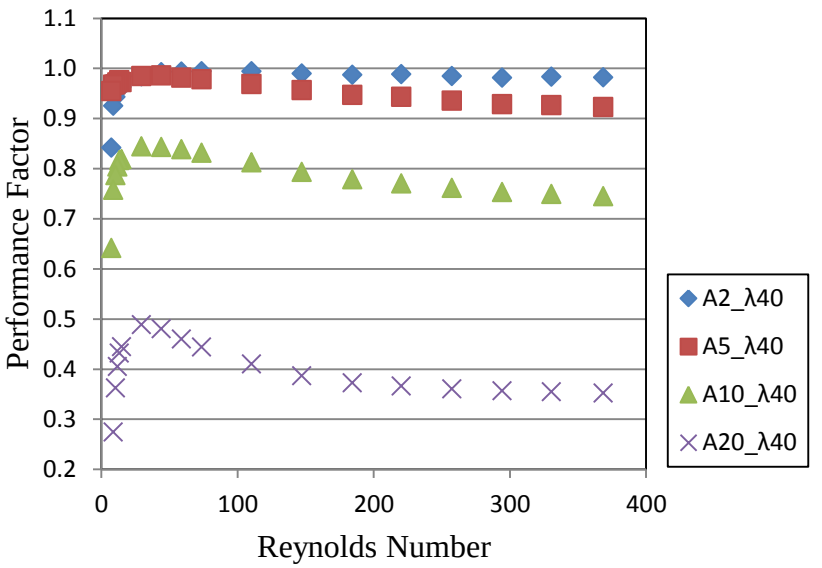

Figure 4.19. Variation in PF with Re for λ =40mm

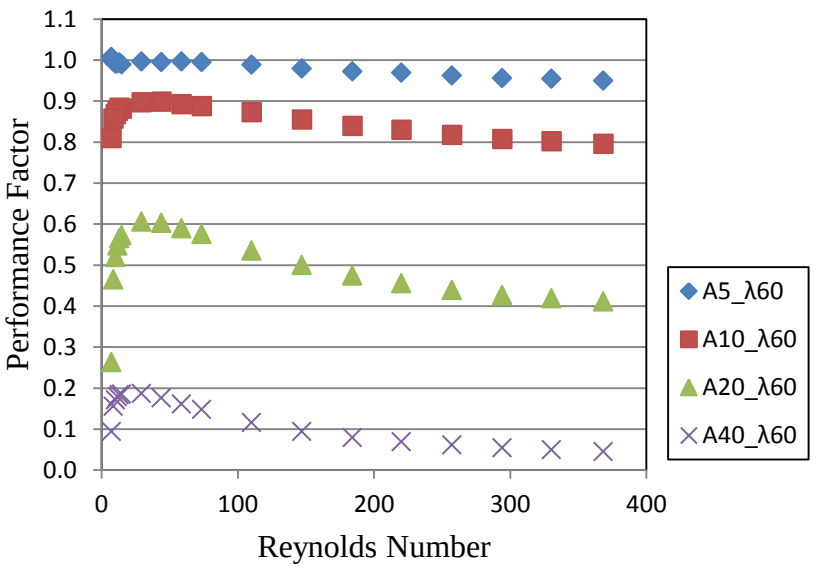

Figure 4.20. Variation in PF with Re for λ =60mm

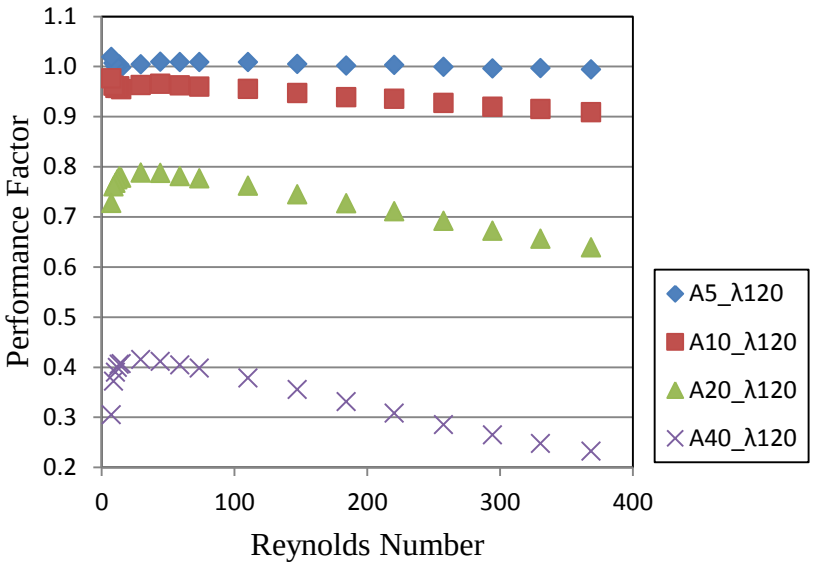

Figure 4.21. Variation in PF with Re for λ=120mm

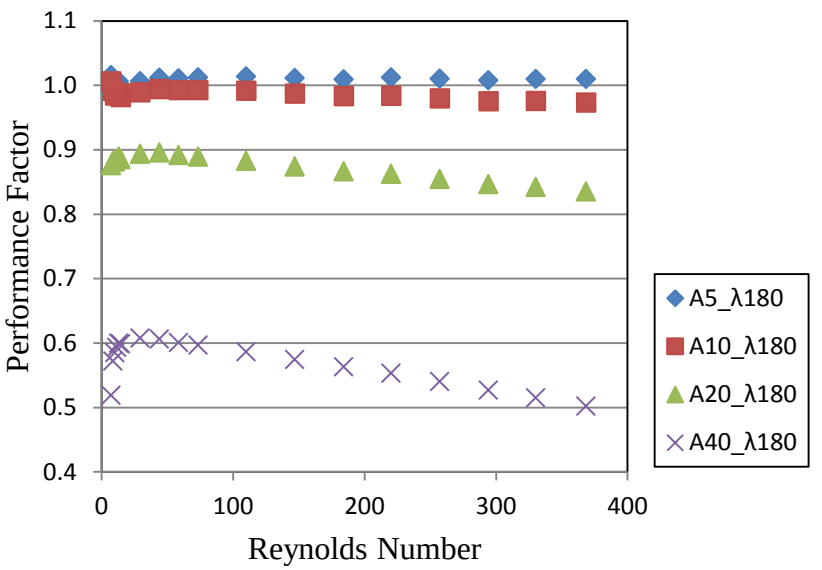

Figure 4.22. Variation in PF with Re for λ=180mm

The numerical results show that the wavy channels do not result in significant increase in PF. There might be a very slight improvement of it at high wavelengths, but even that is very small and it might in the uncertainty of the solution. The wave amplitude (A) is a crucial factor affecting the PF, but it does not affect it positively for all conditions. The positive effect of increase in heat transfer for channels with higher amplitudes is overcome by the more dominant negative effect of increase in pressure drop. Once the results are examined in the figures, an increase in A results in a

decrease of PF. Moreover, the enhancement of overall performance is observed at the lower A values. For some cases, the PF exhibits approximately 2% enhancement such as A=5mm λ=120mm and A=5mm λ=180mm.

4.2.2. Effect of Wavelength

Thermal performance, pump power performance, and the overall performance of the model are investigated for the different wavelengths. These are shown in the related figures.

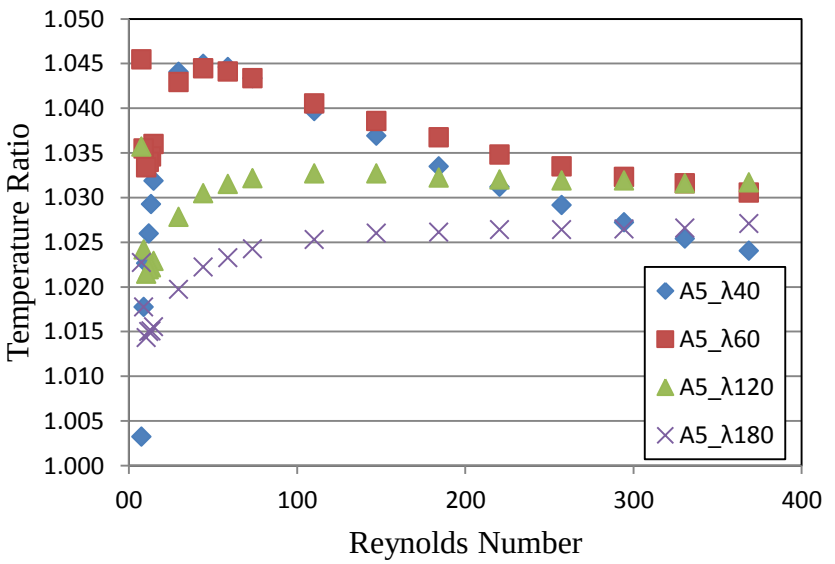

Figure 4.23. Variation in TR with Re for A=5mm

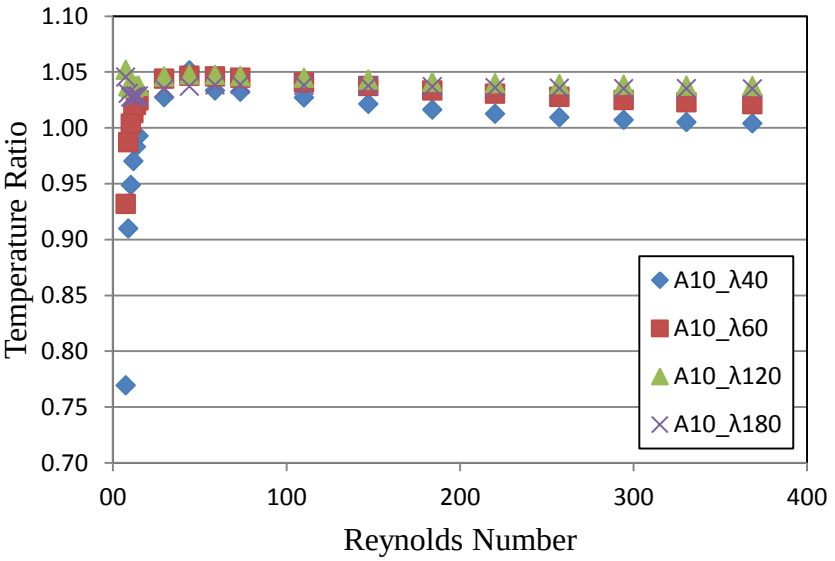

Figure 4.24. Variation in *TR* with Re for *A* =10mm

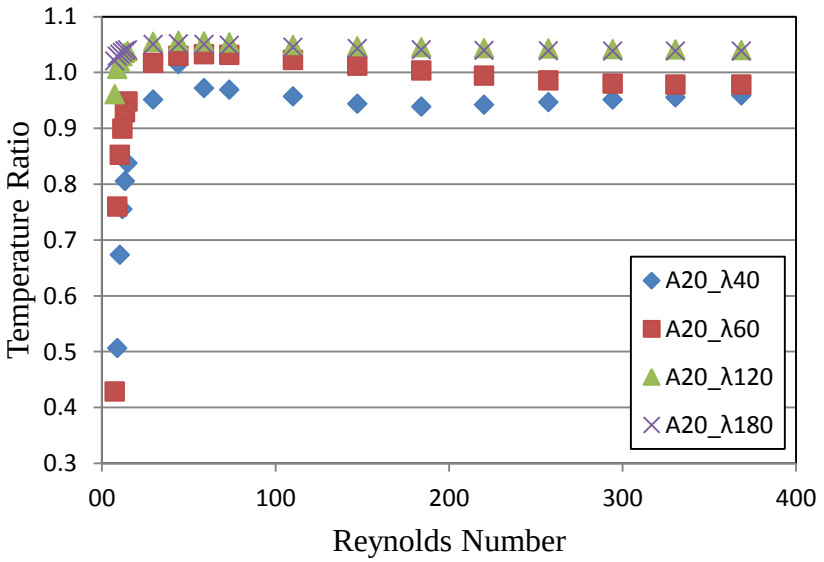

Figure 4.25. Variation in *TR* with Re for *A* =20mm

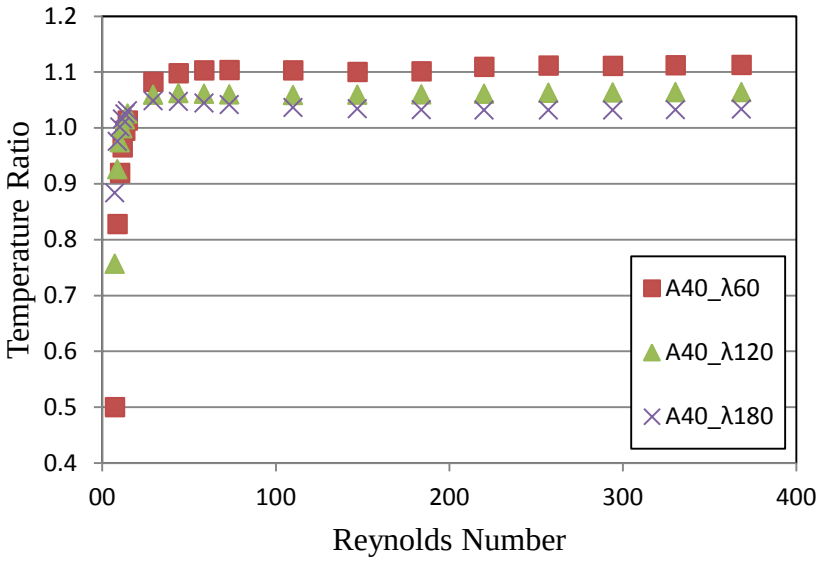

Figure 4.26. Variation in TR with Re for A=40mm

The effect of the wavelength in terms of the thermal performance is shown in Figure 4.23, Figure 4.24, Figure 4.25 and Figure 4.26. The results indicate that especially at lower amplitude, decrease in wavelength causes enhancement of heat transfer. Furthermore, it was found that minimum thermal performance exists for lower λ and Re but the TR is always bigger than 1 for higher λ and Re. In addition to this, TR results are so close to each other for the different λ with various A. Therefore, the effect of λ is not as important for the enhancement of heat transfer as of A.

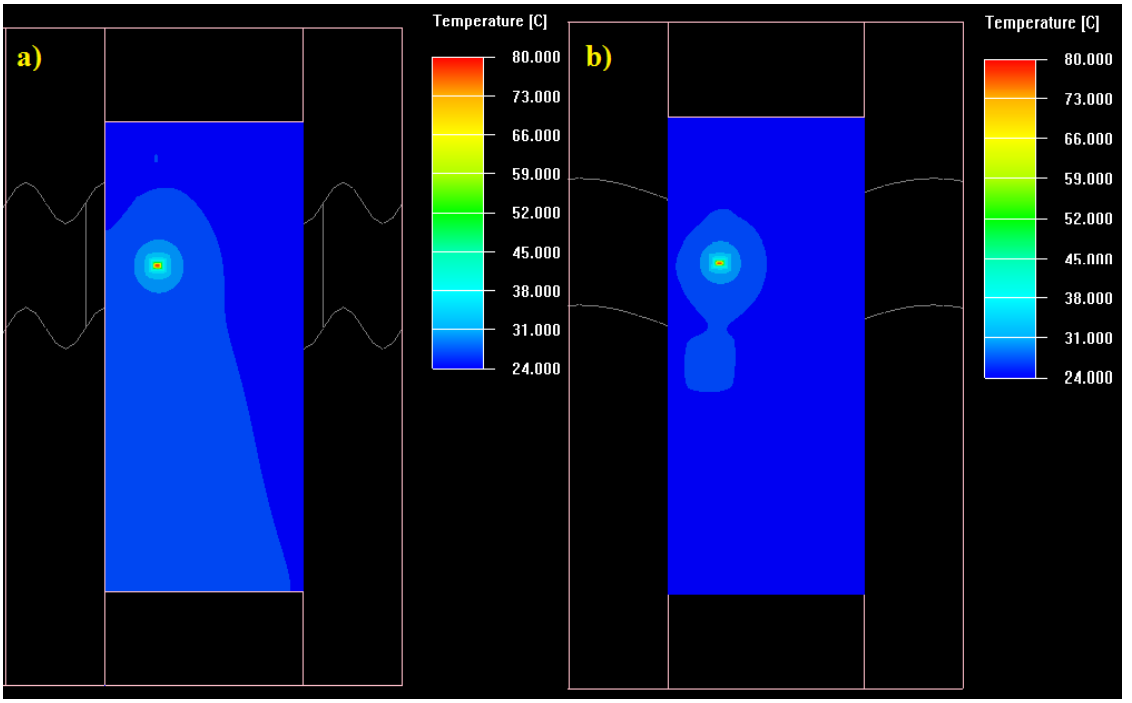

Figure 4.27. Comparison of temperature contours for different wavelengths a) A =10mm λ =40mm b) A =10mm λ =180mm

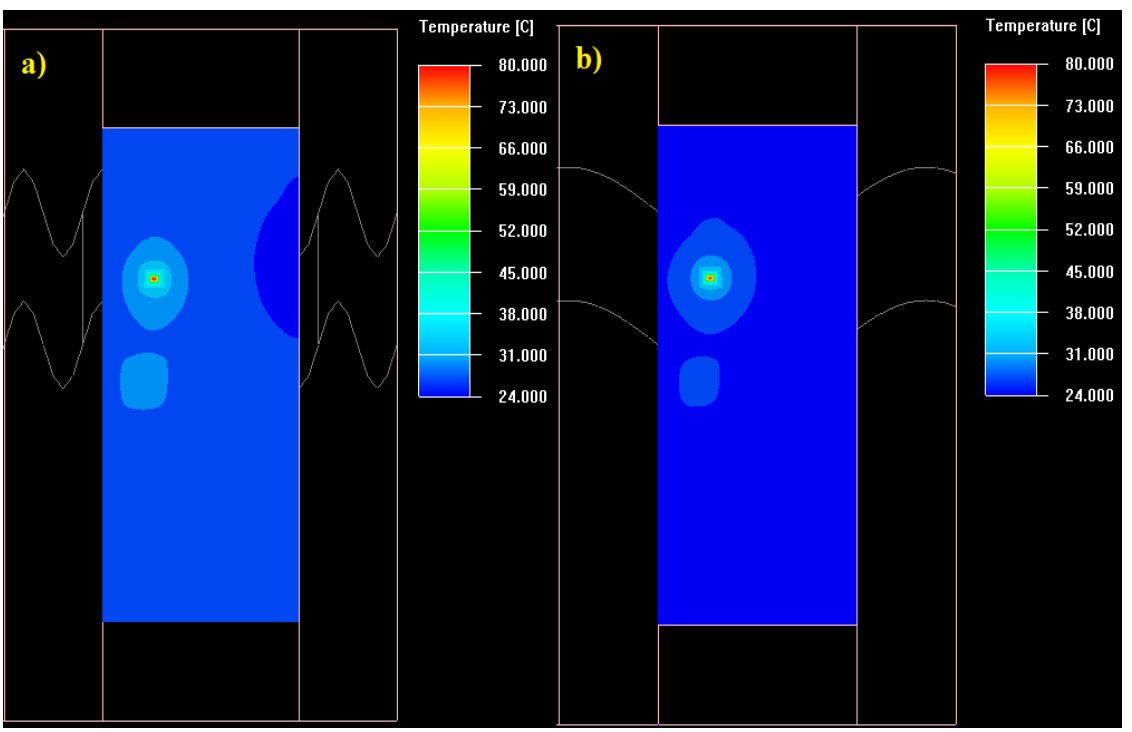

Figure 4.28. Comparison of temperature contours for different wavelengths a) A =20mm λ =40mm b) A =20mm λ =180mm

Figure 4.27 and Figure 4.28 show temperature contours of electronic module surface for different wavelengths.

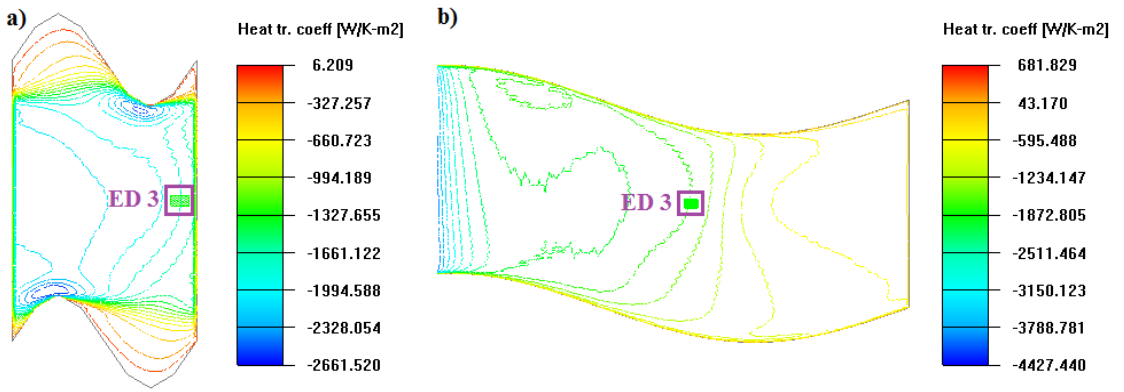

Figure 4.29. Variation of heat transfer coefficient contour line for different wavelengths a) A=10mm λ=40mm b) A=10mm λ=180mm

The heat transfer coefficient contour lines of the channel surface for two different wavelengths are shown in Figure 4.29. Heat transfer coefficient of lower wavelength geometry is bigger than higher wavelength geometry but the difference is very little. Therefore, the wavelength is not very important parameter in terms of heat transfer.

The results of the *WR* are shown in Figure 4.30, Figure 4.31, Figure 4.32 and Figure 4.33.

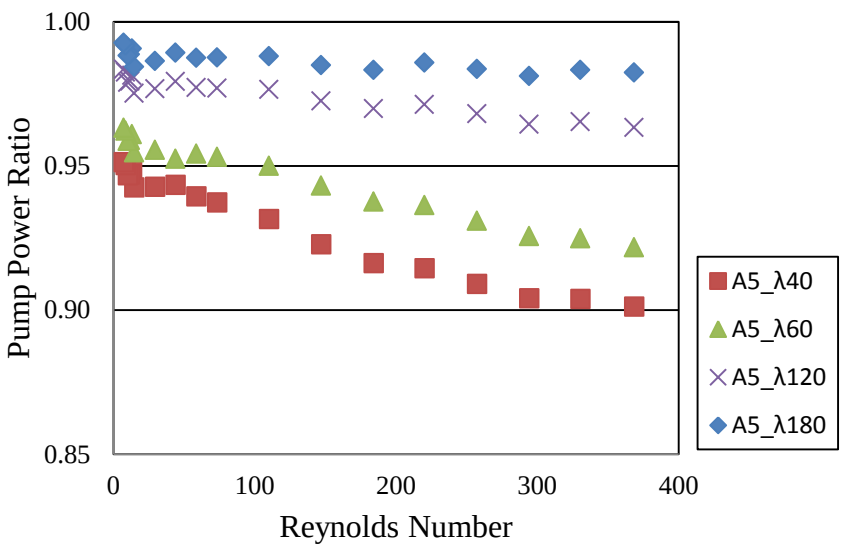

Figure 4.30. Variation in *WR* with Re for A=5mm

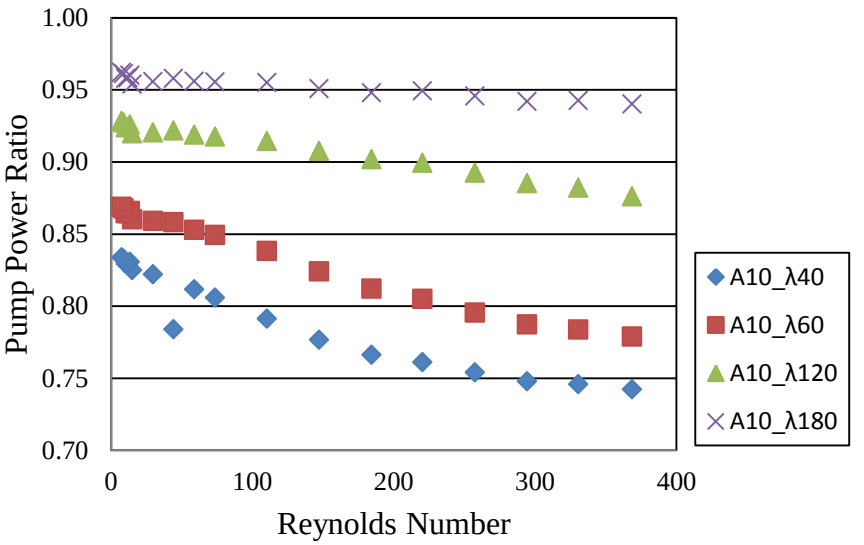

Figure 4.31. Variation in *WR* with Re for *A*=10mm

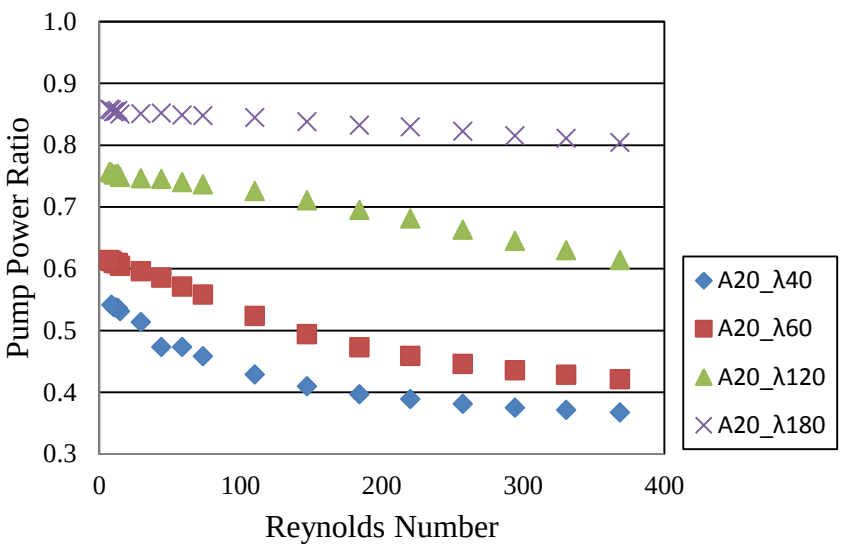

Figure 4.32. Variation in *WR* with Re for *A*=20mm

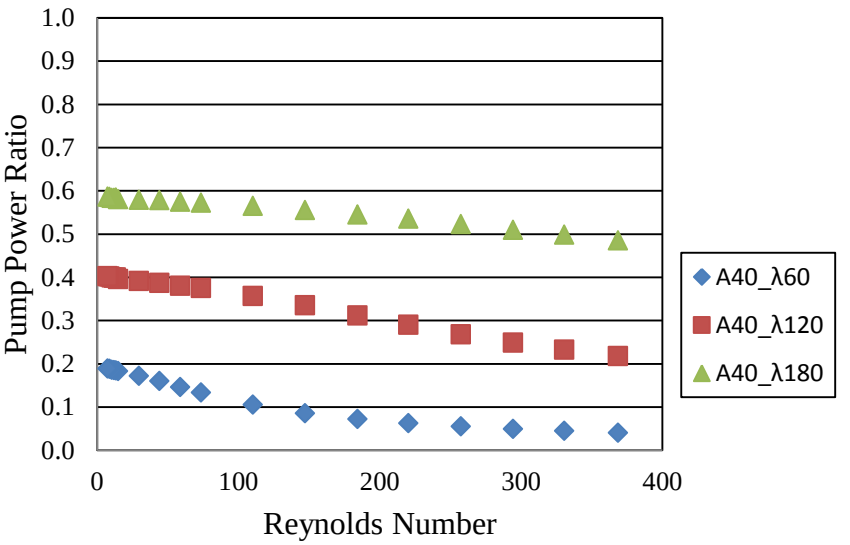

Figure 4.33. Variation in *WR* with Re for A=40mm

The *WR* is smaller than 1 in all results because the pressure drop in the sinusoidal wavy channel is always bigger than the straight channel, however; λ affects the *WR* positively. Once the λ increases which causes to increase the *WR* because of the fact that as λ increases, it makes the channel look more like a straight channel which might be imagined to have a infinitely large wavelength.

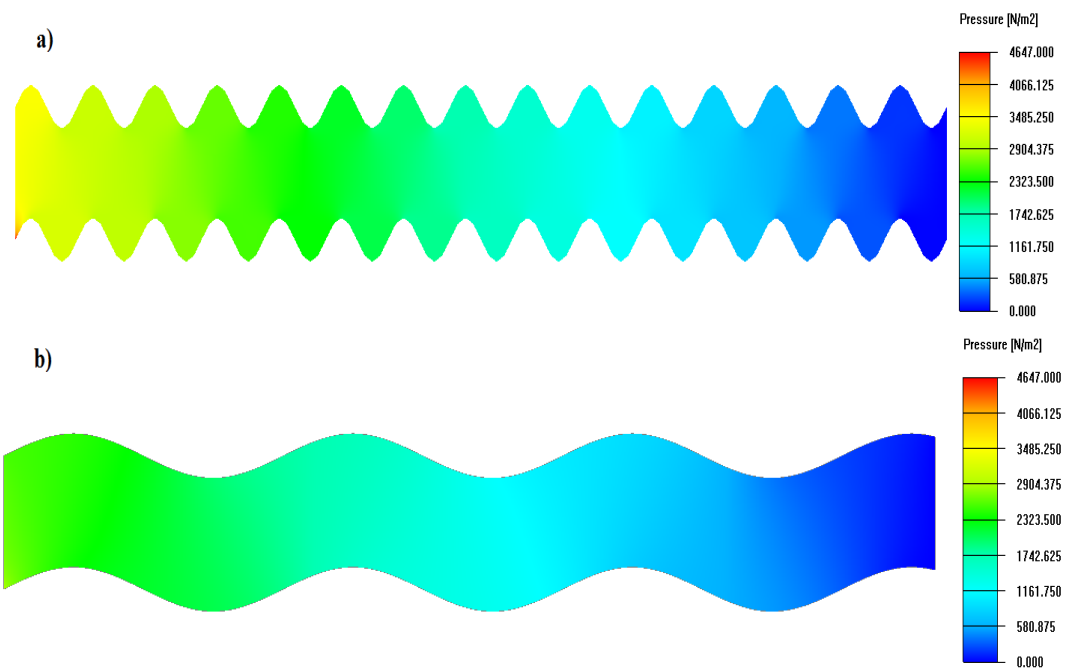

Figure 4.34. Pressure distribution for different wavelengths at Re=368 a) A=10mm λ=40mm b) A=10mm λ=180mm

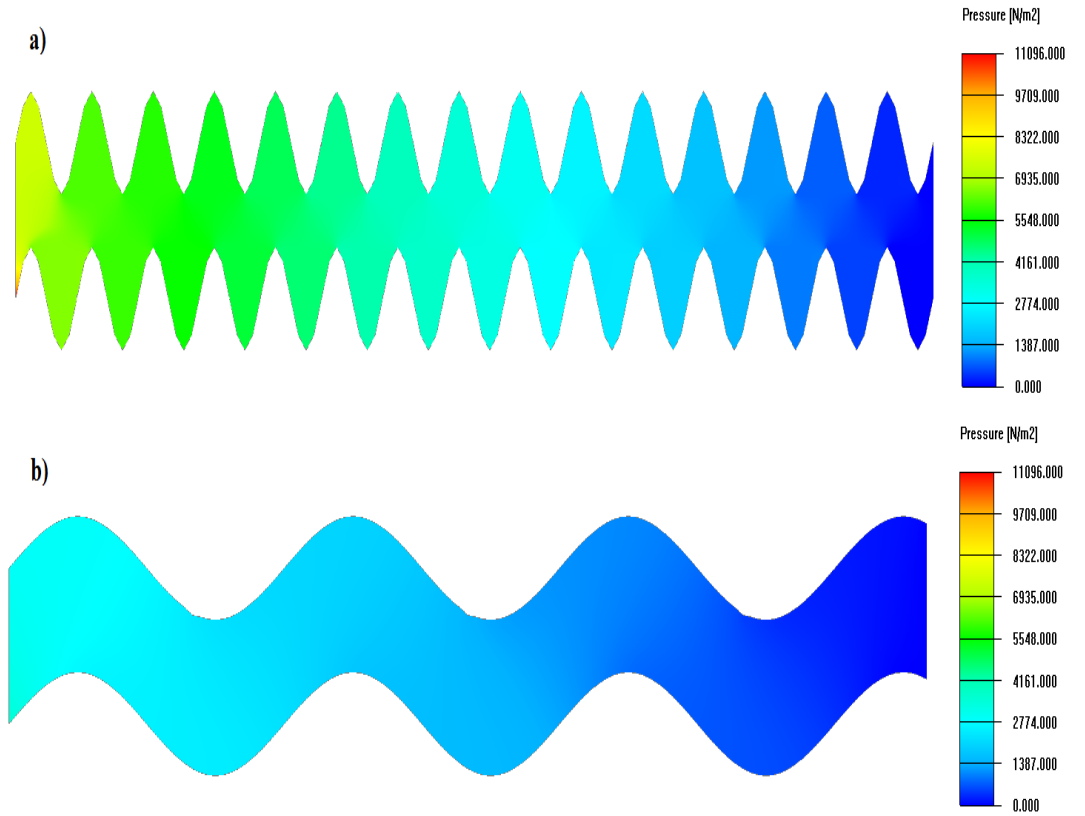

Figure 4.35. Pressure distribution for different wavelengths at Re=368 a) A =20mm λ =40mm b) A =20mm λ =180mm

Pressure distribution contours for different channel geometries are shown in Figure 4.34 and Figure 4.35. Pressure drop in the channel decreases with increasing wavelength. For the geometries in Figure 4.35, the pressure drop value of higher wavelength geometry is approximately three times smaller than lower wavelength geometry.

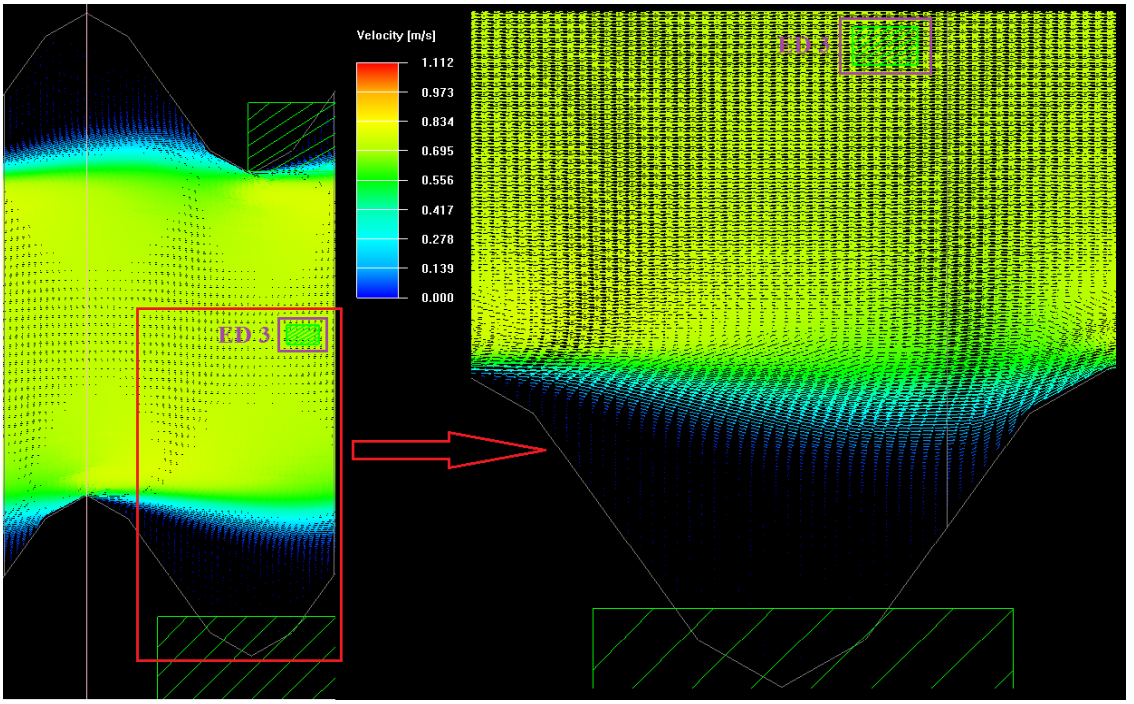

Figure 4.36. Velocity vector for A=10mm λ=40mm at Re=368

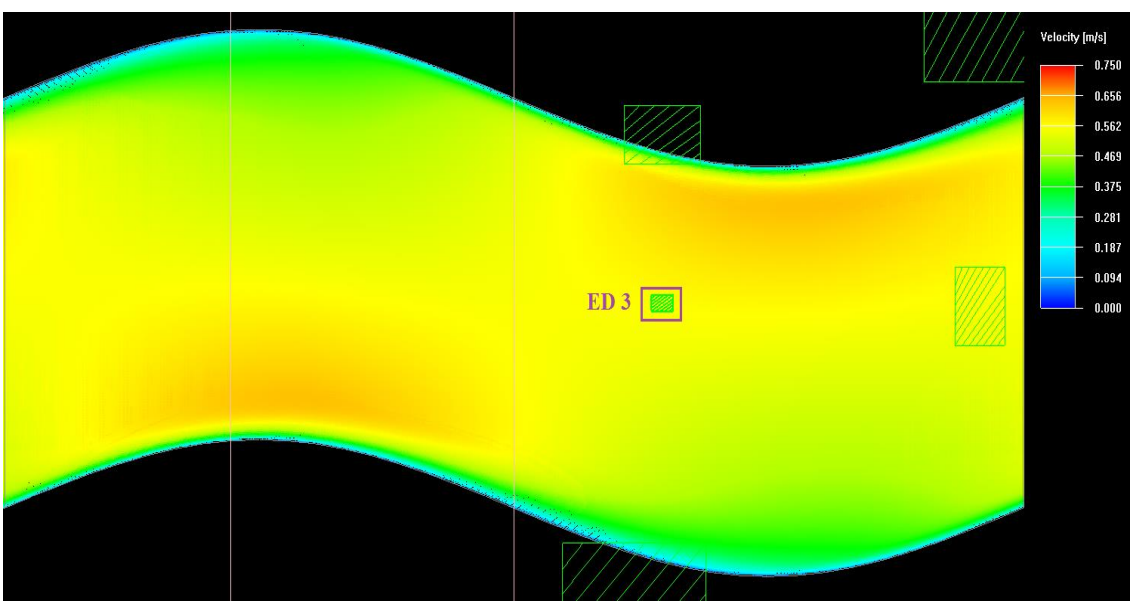

Figure 4.37. Velocity vector for A=10mm λ=180mm at Re=368

Figure 4.36 and Figure 4.37 show velocity vectors for different wavelengths. They indicate that the flow begins to separate from the wall at lower wavelength and causes pressure drop to increase. It can be seen in Figure 4.36.

The results of the PF are indicated in Figure 4.38, Figure 4.39, Figure 4.40 and Figure 4.41 as follows.

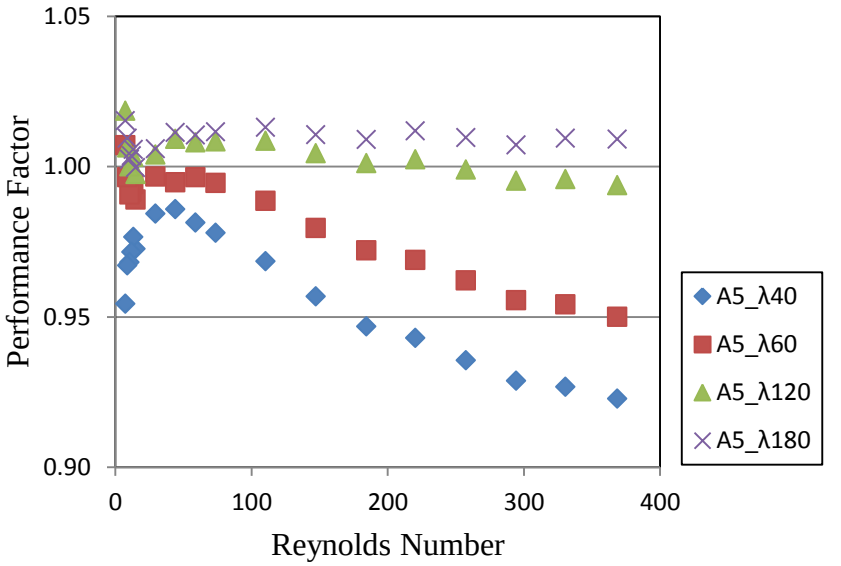

Figure 4.38. Variation in *PF* with Re for *A* =5mm

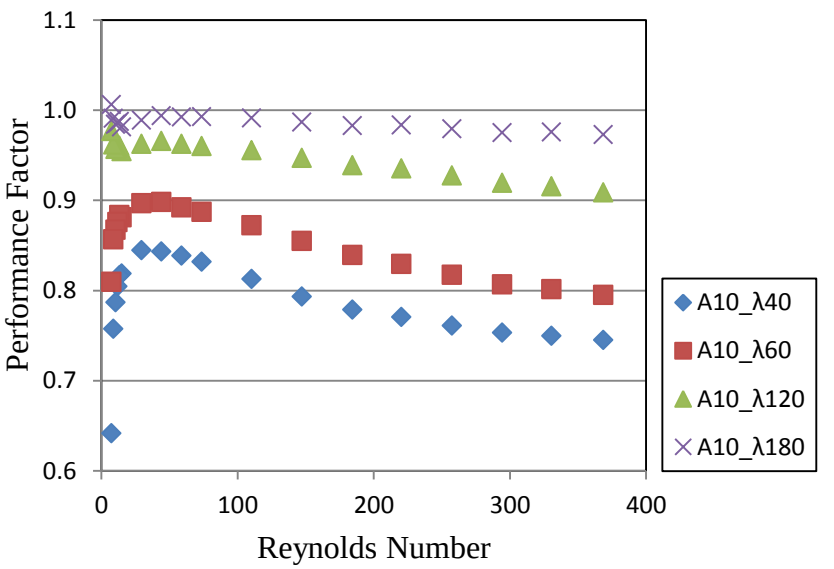

Figure 4.39. Variation in *PF* with Re for *A* =10mm

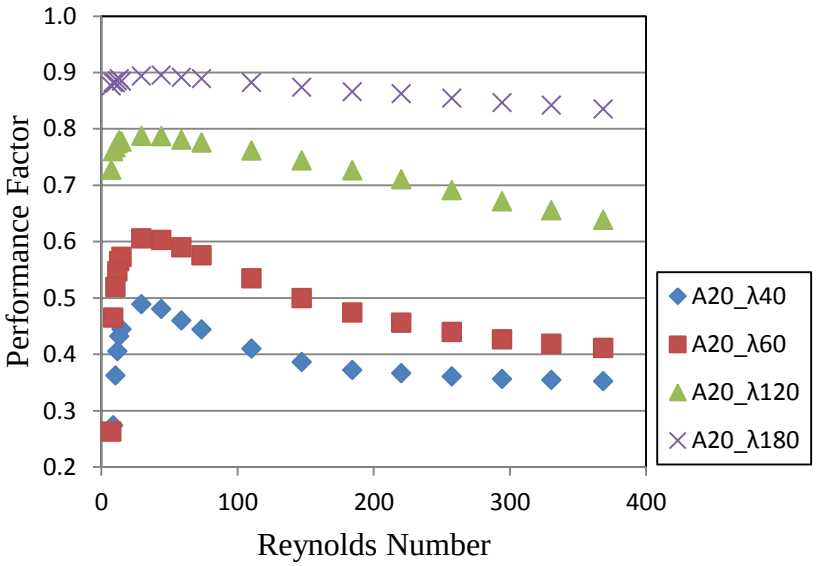

Figure 4.40. Variation in PF with Re for A=20mm

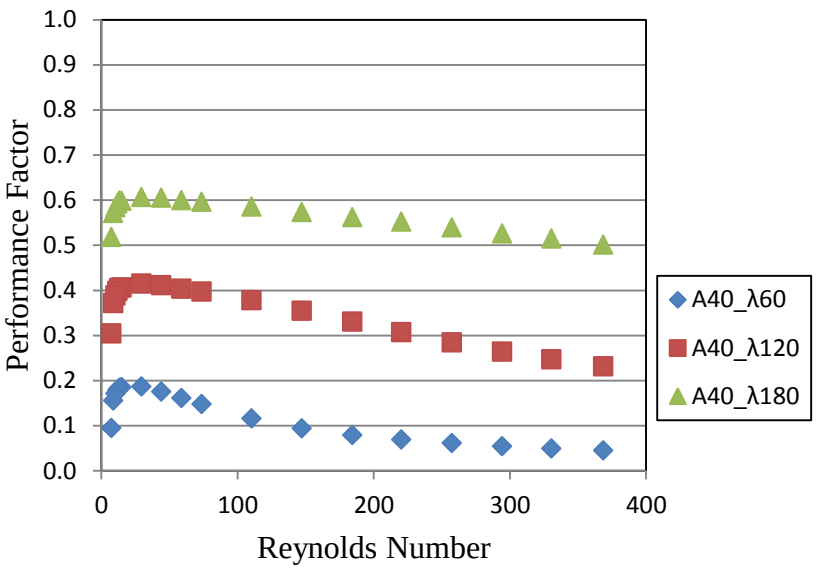

Figure 4.41. Variation in PF with Re for A=40mm

The results show that the increasing wavelength causes the enhancement of the overall performance because this increase of wavelength causes to decrease the pressure drop in the channel. The pressure drop is the dominant factor compared with the heat transfer performance for the PF. Therefore, the wavelength effect can be used for the obtaining different desired cooling conditions.

CHAPTER 5

CONCLUSION

Heat transfer performance and coolant pumping power of sinusoidal wavy channels are investigated numerically in the scope of this thesis, with the purpose of heat transfer enhancement as much as possible while minimizing pressure drop. Reynolds number is changed in the range of 7 and 368. The sinusoidal wavy channels are compared with the reference straight channel. For this purpose, some dimensionless numbers are defined to observe the relative heat transfer performance, pumping power performance and overall performance of geometry. These are *TR* number, *WR* number and *PF* number.

It is understood from these numerical data that, wave amplitude is a much more important parameter for the heat transfer enhancement than the wavelength. The *TR* number usually increases with wave amplitude and Re number. Furthermore, the heat transfer performance of sinusoidal wavy channels are always better than the straight channel, which can be seen the graphs of *TR* number. Some sinusoidal wavy channel geometries shows approximately 10% heat transfer enhancement for A =40mm λ =60mm. At the same time, the increasing in wave amplitude and Re number increases pressure drop in the channel. Therefore, the pumping power of sinusoidal wavy channel is always greater than the straight channel. Increasing of pumping power should be expected when the heat transfer enhancement of sinusoidal wavy channel is utilized in the cooling system. The overall heat transfer performance of geometry is observed by using *PF* number. For some geometries, the *PF* number exhibits approximately 2% enhancement especially at the lower wave amplitudes, but these might be in the uncertainty margin of the data. The best improvement in the overall performance is obtained from A =5mm and λ =180mm. The pressure drop is dominant factor compared with the heat transfer performance for the *PF* number so the minimum pumping power geometry in the study gives the best overall performance.

It must be noted that, wavelength is not important effect in terms of heat transfer for the geometries investigated. An increase in wavelength results in minimization of pumping power because it decreases pressure drop in the channel.

Finally, some future work recommendations might be helpful for better understanding the heat transfer characteristics of sinusoidal wavy channels in cold plate applications;

- Experimental studies must be carried out to make sure about the numerical data.
- The Re numbers must be extended beyond so that a turbulent regime and therefore its effects can be investigated both numerically and experimentally.

REFERENCES

Ansys, Icepak. (2013). R 14.5 Icepak User's Guide.

Bar-Cohen, A, & Kraus, A D. (1983). Thermal Analysis and Control of Electronic Equipment. *New York: McGraw Hill/Hemisphere Publishing Coproration, 2*, 116-123.

Bergles, AE. (1986). The evolution of cooling technology for electrical, electronic, and microelectronic equipment. *ASME HTD, 57*, 1-9.

Cengel, Yunus A. (2007). *Heat & mass transfer: a practical approach*: Tata McGraw-Hill Education.

Fabbri, G. (2000). Heat transfer optimization in corrugated wall channels. *International Journal of Heat and Mass Transfer, 43*(23), 4299-4310. doi: http://dx.doi.org/10.1016/S0017-9310(00)00054-5

Gong, L., Kota, K., Tao, W., & Joshi, Y. (2011). Parametric Numerical Study of Flow and Heat Transfer in Microchannels With Wavy Walls. *Journal of Heat Transfer, 133*(5), 051702-051702. doi: 10.1115/1.4003284

Hossain, M. Z., & Islam, A. K. M. S. (2004). Fully developed flow structures and heat transfer in sine-shaped wavy channels. *International Communications in Heat and Mass Transfer, 31*(6), 887-896. doi: http://dx.doi.org/10.1016/S0735-1933(04)00075-2

Incropera, F. P., Lavine, A. S., DeWitt, D. P., & Bergman, T. L. (2011). *Fundamentals of heat and mass transfer*: John Wiley & Sons Incorporated.

Lytron. (2013). Cold plate catalog. from http://www.lytron.com/~/media/Files/Lytron/Secured%20Files/Quick%20Helpful%20Links/Catalogs/Lytron_Catalog_CP.pdf

Metwally, H. M., & Manglik, R. M. (2004). Enhanced heat transfer due to curvature-induced lateral vortices in laminar flows in sinusoidal corrugated-plate channels. *International Journal of Heat and Mass Transfer, 47*(10–11), 2283-2292. doi: http://dx.doi.org/10.1016/j.ijheatmasstransfer.2003.11.019

Naphon, P. (2007). Heat transfer characteristics and pressure drop in channel with V corrugated upper and lower plates. *Energy Conversion and Management, 48*(5), 1516-1524. doi: http://dx.doi.org/10.1016/j.enconman.2006.11.020

Ničeno, B., & Nobile, E. (2001). Numerical analysis of fluid flow and heat transfer in periodic wavy channels. *International Journal of Heat and Fluid Flow, 22*(2), 156-167. doi: http://dx.doi.org/10.1016/S0142-727X(01)00074-1

Nishimura, T., Ohori, Y., & Kawamura, Y. (1984). Flow characteristics in a channel with symmetric wavy wall for steady flow. *Journal of Chemical Engineering of Japan, 17*(5).

Qu, W., & Mudawar, I. (2002). Experimental and numerical study of pressure drop and heat transfer in a single-phase micro-channel heat sink. *International Journal of Heat and Mass Transfer, 45*(12), 2549-2565. doi: http://dx.doi.org/10.1016/S0017-9310(01)00337-4

Qu, W., Mudawar, I., Lee, S. Y., & Wereley, S. T. (2006). Experimental and Computational Investigation of Flow Development and Pressure Drop in a Rectangular Micro-channel. *Journal of Electronic Packaging, 128*(1), 1. doi: 10.1115/1.2159002

Remsburg, Ralph. (2001). *Thermal design of electronic equipment* (1st ed.): CRC Press.

Rush, T. A., Newell, T. A., & Jacobi, A. M. (1999). An experimental study of flow and heat transfer in sinusoidal wavy passages. *International Journal of Heat and Mass Transfer, 42*(9), 1541-1553. doi: http://dx.doi.org/10.1016/S0017-9310(98)00264-6

Versteeg, H.K., & Malalasekera, W. (1995). *An introduction to computational fluid dynamics the finite volume method* (1st ed.).

Wang, C. C., & Chen, C. K. (2002). Forced convection in a wavy-wall channel. *International Journal of Heat and Mass Transfer, 45*(12), 2587-2595. doi: http://dx.doi.org/10.1016/S0017-9310(01)00335-0